DOI: 10.1002/((please add manuscript number))
Article type: Communication

Ultrastable Supramolecular Self-encapsulated Wide-bandgap Conjugated Polymers for Large-area and Flexible Electroluminescent Devices

Jinyi Lin, Bin Liu, Mengna Yu, Xuhua Wang, Zongqiong Lin, Xinwen Zhang, Chen Sun, Juan Cabanillas-Gonzalez, Linghai Xie, Feng Liu, Changjin Ou, Lubing Bai, Yamin Han, Man Xu, Wensai Zhu, Trevor A. Smith, Paul N. Stavrinou, Donal D. C. Bradley* and Wei Huang**

((Optional Dedication))

Professor Dr Wei Huang, Professor Dr Feng Liu, Dr Jinyi Lin, Dr Changjin Ou, Mr Lubing Bai, Miss Yamin Han, Miss Man Xu, Mr Wensai Zhu
Key Laboratory of Flexible Electronics (KLOFE) & Institute of Advanced Materials (IAM), Jiangsu National Synergetic Innovation Center for Advanced Materials (SICAM), Nanjing Tech University (NanjingTech), 30 South Puzhu Road, Nanjing 211816, China.
E-mail: wei-huang@njtech.edu.cn
Professor Dr Donal D.C. Bradley, Dr Jinyi Lin
Departments of Engineering Science and Physics and Division of Mathematical, Physical and Life Sciences, University of Oxford, 9 Parks Road, Oxford OX1 3PD, UK.
Email: donal.bradley@mpls.ox.ac.uk
Professor Dr Donal D.C. Bradley, Professr Dr Paul N. Stavrinou, Dr Xuhua Wang, Dr Jinyi Lin
Department of Physics and Centre for Plastic Electronics, The Blackett Laboratory, Imperial College London, Prince Consort Road, London SW7 2AZ, UK.
Professor Dr Wei Huang, Professor Dr Linghai Xie, Professor Dr Xinwen Zhang, Dr Bin Liu, Miss Mengna Yu
Center for Molecular Systems and Organic Devices (CMSOD), Key Laboratory for Organic Electronics and Information Displays & Institute of Advanced Materials (IAM), Jiangsu National Synergetic Innovation Center for Advanced Materials (SICAM), Nanjing University of Posts & Telecommunications, 9 Wenyuan Road, Nanjing 210023, China.
E-mail: iamlhxie@njupt.edu.cn
Professor Dr Juan Cabanillas-Gonzalez, Miss Chen Sun
Madrid Institute for Advanced Studies (IMDEA Nanociencia), Ciudad Universitaria de Cantoblanco, Calle Faraday 9, Madrid 28049, Spain.
Professor Dr Trevor A. Smith, Miss Mengna Yu,
ARC Centre of Excellence in Exciton Science, School of Chemistry, The University of Melbourne, Parkville VIC 3010, Australia.
Professor Dr Paul N. Stavrinou
Department of Engineering Science, University of Oxford, Parks Road, Oxford OX1 3PD, UK.
Professor Dr Wei Huang, Professor Dr Zongqiong Lin, Dr Jinyi Lin,
Shaanxi Institute of Flexible Electronics (SIFE), Northwestern Polytechnical University (NPU), 127 West Youyi Road, Xi'an 710072, Shaanxi, China.
Keywords: Ultrastable, Self-encapsulated strategy, Deep blue, Polyfluorene, Flexible electroluminescent devices

Controlling chain behaviour through smart molecular design provides the potential to develop ultrastable and efficient deep-blue light-emitting conjugated polymers (LCPs). Herein, we proposed a novel supramolecular self-encapsulation strategy to construct a robust ultra-stable conjugated polydiarylfluorene (PHDPF-Cz) via precisely preventing excitons from inter-chain cross-transfer/coupling and contamination from external trace H_2O/O_2. PHDPF-Cz consists of a mainchain backbone where the diphenyl groups localize at the 9-position as steric bulk moieties, and carbazole (Cz) units localize at the 4-position as supramolecular π-stacked synthon with dual functionality of self-assembly capability and hole-transport facility. Synergistic effect of the steric bulk groups and π-stacked carbazoles affords PHDPF-Cz an ultrastable property, including spectral, morphological stability and storage stability. In addition, PHDPF-Cz spin-coated gelation films also show thickness-insensitive deep-blue emission with respect to the reference polymers, which are suitable to construct solution-processed large-scale optoelectronic devices with higher reproducibility. High-quality and uniform deep-blue emission is observed in large-area solution-processed films. Electroluminescence shows high-quality deep-blue intra-chain emission with a CIE (0.16, 0.12) and very narrow FWHM of 32 nm. Finally, large-area and flexible PLEDs devices with a single-molecular excitonic behavior are also fabricated. Our supramolecular self-encapsulation design provided an effective strategy to construct ultrastable LCPs for optoelectronic applications.

Flexible polymer light-emitting devices (FPLEDs) are attracted more attentions in industrial and fundamental research for their potential application in wearable equipment, electronic skin and bio-smart devices.[1,2] Beyond the device performance, the improvement of light-emitting conjugated polymers (LCPs) stability has been a long-standing challenge in plastic electronics, which is the main key factor to severely limit the commercialization of solid-state lighting and information displays.[3-7] Compared to narrow band gap (green and red) luminescent molecular materials, the photophysical behavior in wide-bandgap blue LCPs are relatively complicated, involving energy transfer, a large Stokes shift and aggregation-induced excimer emission due to the high-energy absorption and active exciton behavior, which results in poor color purity, low luminescence efficiency and low spectral stability.[8-11] In the last decades, polyfluorenes positioned as an important class of deep-blue LCPs that show pure blue color emission, high luminescence quantum efficiency, and easy processability.[12-14] However, their emission behavior show undesirable features, such as an unstable green emission or strong film thickness-dependent emission, which degrades the color purity and decreases the device efficiency, reproducibility and stability.[2,15-17] To enhance the spectral stability, all types of defects, including chemical and physical defects, should be avoided in polyfluorene solutions and films.[18] Chemical defects are mainly associated to the reactive sites in the aromatic structure, which can facilitate the formation of keto defects following photo or thermal oxidation.[6,17,19] Physical defects include chain aggregates, diverse conformation and superstructures.[6,20-22] All of these defects involve interchain excited states, aggregation-induced energy/charge transfer, non-emissive interchain polaron-pairs, and exciton-exciton annihilation, leading to a stronger lower-band emission or lower emission efficiency due to π-electron delocalization, hybridization and coupling.[7,9,23,24] Technologically, these problems can be partially solved by isolating fluorophores in the solid state through a suitable molecular design.[6] One effective method is to incorporate carbon-bridged fluorenes with steric bulks[25,26] or dendron groups[27,28] into ladder-type polymers to

suppress π-π interactions.[29,30] Another promising strategy is the design of polymers with non-covalent interactions or covalent linkages for the realization of insulated molecular wires (IMWs) by means of molecular encapsulation.[31-37] However, such synthetic procedures are laborious, defects formed by post cyclization of polymer chains lead to steric congestion, and sophisticated threading limits wide application of ultrastable blue LCPs.[33,37] In addition, insulated cyclical encapsulation or large steric frameworks tend to be randomly distributed among the chains in bulky states that significantly affect the interchain charge transport properties,[31,38] which is unfavorable for their application to efficient electroluminescent devices and electrically-pumped lasers.[32,39] A substantial PLEDs performance improving requires LCPs with high photoluminescence quantum yield as well as outstanding charge mobility. It is a challenge for all researchers to realize a careful balance between these conflicting design principles. Herein, we originally propose a supramolecular self-encapsulation strategy, that tethered bulky conjugated polymers with the π-stacked self-assembled units at side chain, is a versatile molecular design tool to achieve such complemetariness (*Scheme 1*A). π-Stacking of aromatic groups located at the side chain assemble into a sheath which surrounds the chain backbone, in analogy with electric power cords, thus serving as "intermediate centers" to enable interchain charge transport and simultaneously to hinder interchain π-π interaction in solid states (*Scheme 1*C).[40,41]

Inspired by the supramolecular steric hindrance (SSH) effect of bulk units on molecular conformation and packing, we proposed a novel strategy based on the molecular integration of steric bulk groups and supramolecular synthons into one functional molecule or chain (*Scheme* 1A).[42,43] For all the effort put into the design of polyfluorenes over the last few decades,[12] the utilization of the fluorene 4,5 position has been completely ignored. Recently, the second planar (*β*) conformational stable polydiarylfluorenes was designed with a balance between the steric interaction of bulky diphenyl (9-position) and the entangled attraction of octyl side chain at 4-poition (van der Waals force, vDW).[22,43-46] Herein, we demonstrate a

supramolecular approach in plastic electronic (Also called Supramolecular Plastic Electronic, SPE) to subtly avoid various pathways for defect generation based on ketone and aggregate formation to construct supramolecular self-encapsulated polyfluorenes. The state-of-the-art model is shortened to PHDPF-Cz, with the incorporation of diphenyl groups as steric repulsors and π-stacked Cz as the attractor at the 4-position (*Scheme* 1B). From theoretical analysis, the diaryl methanene bridge not only suppresses aggregate formation due to the tetrahedral sp^3 carbon configuration but also exhibits the functionality of an antioxidant over the alkyl side chain due to the high bonding strength.[12,16] As expected, the pendent π-stacked Cz group self-assembles into an "encapsulated layer" surrounding the backbone,[47] which hinders the interchain π-π interaction (analogous to the arrangement of electric power cords) and also serves as an "intermediate centre" to allow for interchain two-dimensional (2D) charge transporting (*Scheme* 1C). Therefore, uniform and ultrastable luminescence properties with the single-chain excitonic behavior are observed for large-scale PHDPF-Cz films, which is encouraging for the fabrication of large-area and flexible devices.

π-Stacked aromatic groups based on sp^3 nitrogen are known to show excellent self-assembling and charge transporting behaviour.[40,47-51] In this work, we introduced a π-stacked carbazole (Cz) group into polyfluorene as a pendent steric synthon to fabricate a novel supramolecular bulky wide-bandgap LCPs, PHDPF-Cz (*Scheme* 1B and Figure S1).[12] PHDPF-Cz together with the controlled polymers PHDPF, PODPF, PNDPF and PFO were synthesized following our previous works (*Scheme* S1).[23,45,46] GPC measurements revealed the number-average molecular weight (M_n) of 4.96×10^4 with a polydispersity index (PDI) of 1.65 for PHDPF-Cz, 4.37×10^4 (PDI = 1.68) for PHDPF, 4.74×10^4 (PDI = 1.56) for PNDPF and 5.80×10^4 (PDI = 1.42) for PFO (Figure S2). PHDPF-Cz showed a high decomposition temperature (T_d) of up to 415 °C and glass transition temperature (T_g) of ~168 °C (Figures S3 and S4). The highest occupied molecular orbital (HOMO) and lowest unoccupied molecular orbital (LUMO) energy levels of PHDPF-Cz were estimated to be -2.48 and -5.42 eV via cyclic voltammetry

(CV) analysis (Figure S5).

Firstly, to demonstrate the strong π-stacking interaction of Cz units in the supramolecular self-encapsulated polymer, X-ray diffraction, as well as GIXD of the polymer or monomer were used to visualise the behaviour of the polymer chains. Crystallographic analysis of DBrHDPF-Cz (PHDPF-Cz monomer) gives clear evidence for a π-stacked structural arrangement in which the fluorene monomer is isolated by a Cz "insulated" layer while leaving the terminal bromide groups intact for further modification and polymerization (Figure S6). In addition, as shown in Figure S7, DBrHDPF-Cz in diluted solution showed purple-coloured photoluminescence with a predominant narrow peak in the emission spectrum at a wavelength of 365 nm, which is attributed to light emission from a single Cz unit. Two emission peaks were observed in the PL spectra of a DBrHDPF-Cz single crystal at 390 and 410 nm, which are attributed to partial and full face-to-face intermolecular overlap of Cz groups, suggested strong π-π stacked interaction for the Cz units (Figure S7).[48] This strong π-stacking interaction of Cz units in the monomer crystal implies the possibility for the pendent Cz stacking interaction in PHDPF-Cz in the solid state.

Compared to the non-encapsulated polyfluorenes, PCzODPF has excellent gelation capability in toluene, with a significantly lower critical gel concentration (CGC) of 2.5 mg/ml (0.28% wt, aged 24 hours) at room temperature (Figure S8), indicates that the π-π stacking interaction of pendent Cz moieties is the most likely driving force for PHDPF-Cz/toluene gelation, consistent with the crystallographic analysis of DBrHDPF-Cz discussed above (Figure S6). Besides, circular dichroism (CD) studies were used to demonstrate a positive CD signal for PHDPF-Cz toluene solution or gelation films compared to no CD signal observed in non-gelatin solvent ($CHCl_3$) solution where PHDPF-Cz is molecularly dissolved (Figure S9). Films coated from $CHCl_3$, as well as all controlled PNDPF films, also showed no CD effects, and confirmed that the self-assembled gelation structure of PHDPF-Cz has a helical property. In practice, this molecular gelation structure in “precursor” hydrocarbon solutions may

propagate into the mesoscale morphology of a spun film, particularly when only chain swelling occurs in the absence of non-covalent interactions between chain and solvent molecules.[12,20,22,45,52] As shown by the AFM images in Figures S10-S15, in contrast to the smooth surfaces found in the controlled polymer films, the "likely" oriented nanostructure can be obtained in PHDPF-Cz films spin-coated from toluene solution. Grazing incidence X-ray diffraction (GIXD) is also applied here to characterize the interchain π-π interaction and chain behaviour of PHDPF-Cz, PODPF, PNDPF and PHDPF spin-coated films. In general, the GIXD images clearly show a continuous diffraction ring and no obvious patterned spots, which indicated that all materials are in completely amorphous states. The corresponding diffusive ring with a broad peak at Q_{xy} = 1.325~1.378 $Å^{-1}$ (d = 4.557~4.740 Å, from $d = 2\pi/q$) and Q_z = 1.423~1.433 $Å^{-1}$ (d = 4.413~4.382 Å) may be ascribed to the interchain π-π interaction (chain aggregation in all controlled films) (Figures S10-S15). However, for the PHDPF-Cz film spin-coated from toluene solution, no obvious diffraction ring was observed for the Q_{xy} (from 1.300~1.400 $Å^{-1}$) direction in the GIXD pattern image, indicating extremely weak or even no interchain π-π interaction (d > 4.740 Å, Figure S12). The fairly intense peak at Q_z = 1.382 $Å^{-1}$ is ascribed to the distance between the steric carbazole moieties (d_{Cz} = 4.544 Å, *Scheme* 1c and Figure S12), similar to previous work.[47] Intuitively, the results shown above further confirmed weak interchain π-π interaction in the PHDPF-Cz films spin-coated from toluene, which leads to the realization of remarkable intrachain photophysical properties in the absence of interchain excited states in the solid state.

Ideally, our supramolecular self-encapsulation approach enable PHDPF-Cz to show excellent intrachain photo-physical properties in the solid state.[25,31,32] One can expect reduced energy transfer and quenching aggregation processes to result in a very small red-shift of the PL spectrum in films compared to that in solution.[36,53] The PL spectrum of PHDPF-Cz in toluene solution (10^{-3} mg/ml) consisted of three emission peaks at 434, 458 and 491 nm, attributed to the 0-0, 0-1 and 0-2 vibronic transitions of a single polyfluorene chain (Figure 1).

Interestingly, the PL spectral shape of a PHDPF-Cz spin-coated film was very similar to the PL measured in solution (Figure 1A), with a slight red-shift of approximately ~4 nm (438, 461 and 495 nm) observed. These small peak shifts, which we could not assign to any particular feature of conventional "IMWs", are probably due to solvent effects, where restriction of the conformational motion and/or dielectric constant leads to changes in the solid films. Importantly, PHDPF-Cz gelation samples showed similar emission peaks but with a slightly larger 0-1/ 0-0 peak ratio compared to solution and the spin-coated film. This can be reasonably explained by the stronger self-absorption shown by thicker samples. Conversely, PFO, PODPF, and PPFOH gels show different PL spectral shapes when processed in any of the mentioned forms, which is mainly assigned to stronger aggregation and interchain π-π interaction.[20,21,45] In addition, the intrachain emission properties of PHDPF-Cz solution and gels were further investigated by time-resolved PL measurements (Table S1). Typical PHDPF-Cz gels showed a PL decay lifetime of 466 ps at 440 nm, 486 ps at 468 nm and 491 ps at 499 nm, which are nearly the same as in diluted solution for the emission peak of 433 (472 ps), 460 (486 ps) and 480 nm (480 ps), with only one component (Figure S16), which are all significantly different from those obtained for PFO.[38] These data stronger supported that there is weaker π-π interaction of backbone chain and the absence of interchain excited states in the gelation structure. Moreover, the fluorescence quantum yields (PLQY, Φ) of PHDPF-Cz in solution and pristine film are ~80% (±5) and ~55% (±5), respectively, which are slightly higher than that found for the controlled polymers, retaining 71% of the value in solution ($\Phi_{film}/\Phi_{solution}$). Similar $\Phi_{film}/\Phi_{solution}$ ratios are found in conventional IMW films that have been highlighted as solid-state emissive materials in the literature.[35]

More interestingly, the PL spectral shape of PHDPF-Cz pristine gelation films is independent of film thickness from 60 to 155 nm (Figures 1B and S17) due to the screening effect of the "insulation". This thickness-insensitive PL property is very important for industrial applications and can be used to enhance the reproducibility of device performance and

fabrication via large-scale print processing. Conversely, the intensity ratio for the 0-1/0-0 band emission for a PHDPF-Cz film spin-coated from $CHCl_3$ solution is slightly enhanced with increasing film thickness, which may be attributed to weaker intrachain and interchain *JH*-aggregation behaviour in the solid state.[3,53] Note that we cannot completely avoid the self-absorption effect in the thick film samples (Similar absorbance intensity of PHDPF-Cz and PHDPF with the same film thickness as shown in Figure S18). For the controlled polymers, the emission spectra of PHDPF and PNDPF pristine thin films (thickness of 90~100 nm) showed three peaks at 443, 463 and 493 nm, but the intensity of the emission peak at 463 nm (0-1 band) was stronger than that at 443 nm (0-0 band).[54] Moreover, PL spectra of PHDPF, PODPF and PNDPF pristine films were strongly influenced by the film thickness from 60 to 150 nm (Figures S17), which also confirmed strong interchain aggregation, consistent with the GIXD and NMR results.[3] Due to the screening effect of the insulation, the optical properties of PHDPF-Cz films are only slightly sensitive to the solution processing conditions, film morphology and thickness. Therefore, a large-scale high-quality PHDPF-Cz film (30 cm × 10 cm) deposited onto a flexible PET substrate using a scraping method showed PL similar to that found for the spin-coated film, with a uniform deep-blue emission under 365 nm UV light excitation (inset shown in Figure 1B).

Subsequently, we also demonstrated a systematic visualization for this single-chain excitonic behaviour in PHDPF-Cz and PHDPF films via ultrafast time-resolved spectroscopy (Figures 1C-1F). Novel time-resolved scanning confocal fluorescence imaging (FLIM) measurements are explored here to investigate excitonic behaviour in solid states. As discussed above, a uniform and smooth PHDPF film was obtained by spin-coating from toluene solution. As shown in Figure 1C, a relatively homogeneous morphology was observed in FLIM images collected from typical regions in this film for the completely amorphous states. The major lifetime of the PHDPF exciton in this film was approximately 308~450 ps, with an average value of 380 ps, consistent with the values reported for polyfluorene solutions and spin-coated

films. However, for the PHDPF-Cz film obtained from toluene solution, increased roughness was observed, which is attributed to the formation of oriented nanostructures. The morphology of the films, in particular the presence of relatively inhomogeneities in the fluorescence decay behaviour on the submicro- or nanometer scales (Figure 1C), is clear, similar to the results of AFM analysis. Meanwhile, the exciton lifetime was measured to be much shorter (150~300 ps, average value is about 190 ps). According to the Franck-Condon principle, these striking differences in band shape, suggested the slightly different geometry between the excited state and the ground state observed for the case of the Cz-threaded layer.[36] Weakly emissive π-π stacked strands can suppress ultrafast exciton transferred into non-emissive inter-chain polaron-pairs, which can decrease the exciton decay time. In fact, chain separation induced by the self-encapsulation in PHDPF-Cz also suppresses exciton-exciton annihilation, which is usually happened in densely packed condensed structure. Figures 1D and 1E show the pump-probe transient absorption spectra of PHDPF and PHDPF-Cz spin-coated films which contain spectral signatures of stimulated emission (SE) and photoinduced absorption (PA). Below 2.4 eV (517 nm), PHDPF and PHDPF-Cz films exhibit strong SE bands confirming their emissive and light amplification capabilities, being promising candidates as optical gain media in lasers. In line with PFO, the PA signal in PHDPH and PHDPF-Cz is expected to have two different components: a PA band in the 520-540 nm spectral region arising from polaron pairs and a singlet exciton PA band extending towards the red-NIR, both having different kinetics. Figure 1F depicts a comparison between SE and PA dynamics at 603 and 611 nm (the wavelength where polarons supposedly have the larger spectral contribution) in both polymers. Starting with PHDPF-Cz, SE and PA dynamics follow parallel trends suggesting the dominant interplay of intra-chain singlet excitons and the lack of polaron states at long time delays. Conversely, in PHDPF film, SE at 2.7 eV (462 nm) clearly exhibits a much shorter-lived component absent in PA at 2.06 eV (602 nm). These discrepancies seen to confirm that the polaron pair yield is much higher in PHDPF than in

PHDPF-Cz upon same photoexcitation conditions.[55,56] Recently, Sun et al. reported on a suppression of polaron features in the transient absorption spectra of thiophene-based IMWs films, which they assign to hindrance of inter-chain hole / electron transfer required to stabilize polaron pairs.[57] Accordingly, chain isolation promoted by Cz stacked layers in PHDPF-Cz could contribute to effectively encapsulate excitons and reduce the exciton dissociation probability. Our molecular design enables the suppression of induced absorption associated with long-lived excited states by inhibiting inter-chain aggregation, while further enhancing the emission properties of LCPs.

Compared to the conventional thermal stability and working stability of LCPs, the storage stability of LCPs films has been rarely addressed in the last several decades, which is the most important factor determining practical optoelectronic application in the future. Molecular encapsulation of the conjugated backbone can also significantly improve the chemical stability.[31,58-60] In previous studies, the stability of LCPs was analysed by thermal annealing and DSC recycling.[12,18] Note that it is not enough to only evaluate the chemical, morphological, or spectral stability, especially to check the storage and working stability of materials and devices. Similar to other reported highly stable polydiarylfluorenes, PHDPF-Cz, PHDPF, PODPF and PNDPF films showed excellent spectral stability after thermal annealing at 180 °C under ambient conditions for 10 min (Figures 2A, and S19).[45] Increased thermal annealing temperature or ageing time led to the observation of weaker green-band emission in common polydiarylfluorenes without Cz units. The corresponding I_{green}/I_{blue} (ratio of light emission intensity at 555 nm and 440 nm) is approximately 0.35 (2 h) (initial value is about 0.07). Interestingly, our novel self-encapsulated PHDPF-Cz showed excellent thermal spectral stability, with an I_{green}/I_{blue} value of 0.08 after annealing for 8 h (initial value was approximately 0.05). Besides, the 3D AFM image of the PHDPF-Cz pristine film also showed some nanostructure. In addition, instead of larger aggregates or domains, we found a slightly smoother morphology in all annealed films, which indicates excellent thermal morphological

stability (Figure 2A). However, the thermally annealed PHDPF films showed some obvious aggregate formation and crystalline superstructure, consistent with our previous work.[22] However, evaluating the stability via thermal annealing is extremely not enough. Therefore, we also aged the pristine films in air for about 21 days, and, in some cases, even longer (room temperature, R.H.: 70%, daylight and even under UV irradiation, Figure S20) and observed that all PL spectra of the PHDPF and PNDPF films changed conspicuously with the appearance of an additional shoulder of green (g)-band emission at 555 nm (Figure 2B). The corresponding light emission colour of PHDPF and PNDPF films changed from deep-blue to green-yellow. Remarkably, PHDPF-Cz films spin-coated from toluene solution showed excellent stability, with no obvious g-band emission observed under the same ageing conditions and even greater stability than films spin-coated from $CHCl_3$ solution that showed a weaker g-band emission at 555 nm and a stronger 0-1 band emission. The green indices I_{green}/I_{blue} are approximately 0.75 and 0.45, 0.60 and 0.62, and 0.10 and 0.05 for PNDPF, PHDPF and PHDPF-Cz aged films spin-coated from $CHCl_3$ and toluene solutions, respectively. As expected, all β conformation and amorphous PFO films showed stronger g-band emission after ageing for 3 days under the same conditions (Figure S21), with the corresponding I_{green}/I_{blue} ratio being approximately 0.48 (DCE), 1.55 (Toluene) and 1.85 ($CHCl_3$). These results indicated that PHDPF-Cz shows an advantage over PNDPF, PODPF, PHDPF and PFO in terms of improved film spectral stability. However, the Φ of all our films decreased with prolonged aging time, as shown in the inset of Figure 2C. Pristine films processed under the same conditions but stored in a N_2 atmosphere glove box showed no g-band emission, which suggested a synergistic effect of H_2O and O_2 on g-band emission (Figure S22). Besides, we also observed that there is no obvious change in the absorbance spectra of all polymers spin-coated films in this work after thermal annealing aging in the air several days (Data not shown here). The mechanism for the instability (also called photobleaching) has not yet been elucidated, but whatever process is involved, the control

PFO, PHDPF and PNDPF films show lower photostability under mixed H_2O/O_2 and light. The discovery that the supramolecular self-encapsulation can significantly improve the fluorescence and photostability of PHDPF-Cz indicates that this may be a valuable method for enhancing the stability and brightness of LCPs.

Conventional architectures for IMWs with the encapsulated framework served as so-called insulated "dopants" with steric hindrance, tended to be randomly distributed within the conjugated chain, and showed extremely lower transport properties that were strongly affected by the resulting structural and electronic disorder[31,36] (such as the incorporation of cyclic side chains, which decreased the carrier mobility from 4.8×10^{-5} to 4.7×10^{-11} cm^2 V^{-1} s^{-1},[39] for example). In this regard, such "IMWs" bulky film may not be suitable for efficient electroluminescent devices and electrically pumped lasers. In sharp contrast with the insulated encapsulated layer used in these reported IMWs, use of π-stacked Cz groups as a threaded "encapsulated layer" in our system probably not only suppresses interchain energy transfer and facilitates single-molecular excitonic behavior but also enables two-dimensional (2D) coherent charge transport (both π-conjugated and π-stacked channel[48,61]) with comparable charge mobility (*Scheme* 1C). Firstly, we fabricated hole-dominated devices (ITO/PEDOT:PSS/polymers/MoO_3/Au) to investigate the transport capability of PHDPF-Cz. As shown in Figure 3A, the hole mobility of PHDPF-Cz films spin-coated from $CHCl_3$ solution is slightly dependent on the film thickness and is approximately 10^{-5}~10^{-4} cm^2 V^{-1} s^{-1} for a root square of the electrical field $E^{1/2}$ in the range of 400~600 $(V/cm)^{1/2}$, similar to PFO and PODPF films.[13,44,62] In addition, the hole mobility of PHDPF-Cz MWs films clearly shows a thickness dependence, with values of approximately 10^{-6}~10^{-4} cm^2 V^{-1} s^{-1} under the same conditions, which is comparable to the hole mobility reported for conjugated polymers with stronger π-π interaction.[39,63] Although the rough surface morphology of PHDPF-Cz film may lead to slightly lower mobility values than those found for films spin-coated from $CHCl_3$ solution, this mobility is several orders of magnitude higher than that previously reported for

spin-coated IMW films.[38] For our novel PHDPF-Cz film, Cz units incorporated into the side-chain do not only disturb the π-stacking of the polymer backbones but also act as an "intermediate centre", which enables hole charges to delocalize across different chains sufficiently to exhibit the signatures of 2D coherent transport, as discussed above (*Scheme* 1C). As a consequence, given the importance of charge carrier balance, the hole mobilities observed are likely to be beneficial for realizing high values for the electroluminescence quantum efficiency. PLEDs with a sandwich structure composed of ITO/PEDOT: PSS/polymer films with varying film thickness/TPBi (30 nm)/LiF (0.5 nm)/Al (100 nm) were fabricated (Figures 3 and S23-30). As shown in Figure 3B, the EL spectra of PHDPF-Cz devices consisted of three emission peaks at 440, 461 and 495 nm, with a full-width at half-maximum (FWHM) of 32 nm, which is strikingly similar to the corresponding PL spectrum. As the applied voltage was increased from 4 (0.072 mA cm^{-2}) to 9 V (218.3 mA cm^{-2}), devices showed stable deep blue emission, with CIE coordinates of (0.16, 0.12). Moreover, owing to the absence of interchain energy transfer, the EL spectra of PHDPF-Cz-based PLEDs are independent of emissive film thickness (Figures S23-25). Conversely, the EL spectra of PHDPF pristine films (92 nm) showed a maximum peak at 470 nm, together with emission peaks at 443 and 495 nm, with a full-width at half-maximum (FWHM) of 72 nm and a CIE of (0.20, 0.21) (Figure S28). However, the 0-1 band emission peak decreased in the EL spectra measured for PHDPF pristine films with decreasing thickness from 92 to 58 nm (Figure S29). These thicknesses (morphology)-dependent EL spectra are undesirable for improving device reproducibility and stability. Devices based on PHDPF-Cz films spin-coated from toluene solution showed a lower turn-on voltage of 3.95 V and a maximum brightness of 3523 cd m^{-2}, with a luminous efficiency of 2.56 cd A^{-1} (Figure 3C). In addition, devices based on PHDPF-Cz films spin-coated from toluene outperformed devices based on films processed from $CHCl_3$ as well as devices based on PHDPF, which demonstrates the improved emission stability.

Excellent deep-blue spectral and morphological stability with a relatively narrow FWHM of 32 nm for the light output can enable fabrication of larger-scale flexible PLEDs. Therefore, flexible large-scale PLEDs were also fabricated based on a flexible substrate configuration of (PET) (75 μm)/PEDOT:PSS electrode layer (30 nm)/ PEDOT:PSS (80 nm)/PHDPF-Cz layer (110 nm)/Ca (30 nm)/Al (120 nm). The total area for the flexible devices is approximately 8 × 8 cm, with two different cell sizes of approximately 30 mm × 2 mm and 10 mm × 2 mm. The transparent electrode is also based on a commercially available PEDOT:PSS formulation. The PHDPF-Cz film thickness is approximately 105~125 nm. Finally, an Al electrode is used to form the back contact. The flexible PLEDs show a luminance of 1000 cd m^{-2} at 8.2 V, with the highest luminance obtained of 1780 cd m^{-2} and a power efficiency of 1.73 cd A^{-1}. The devices are fully functional PLEDs, with reasonable operating conditions of $<$5 V turn on voltage (4.55 V). Finally, PL and EL spectra of PHDPF-Cz solution, gel and films with varying thicknesses (pristine, annealed, and aged in air) are remarkably similar (Figure 3D), strongly supporting the validity and effectiveness of the supramolecular self-encapsulation strategy. Therefore, our self-encapsulated polymer demonstrates excellent electroluminescent properties, which can be exploited for plastic-based flexible displays.

To summarize, we have implemented a supramolecular self-encapsulation strategy for controlling interchain interactions of LCPs in the solid state via tethering the backbone chain with supramolecular π-stacked layers. An excellent gelation property of PHDPF-Cz in toluene solution indicated a strong π-π stacking interaction of Cz groups. Therefore, pendent Cz groups can self-assemble into a protective sheath, not only to inhibit interchain interaction and afford intrachain emission behaviour but also to improve spectral and morphological stability and interchain charge transport. Finally, stable deep-blue PHDPF-Cz-based PLEDs with EL featuring the intrachain excited state, can be fabricated with a high current efficiency of 2.56 cd/A and low turn-on voltage of 3.95 V. The fabrication of larger-scale and efficient flexible PLEDs further confirmed the effectiveness of our supramolecular self-encapsulation strategy.

Supporting Information
Supporting Information is available from the Wiley Online Library or from the author.

Acknowledgements
We thank primary financial supports by the National Natural Science Foundation of China (61874053, 21504041, 21502091), the National Key Basic Research Program of China (973) (2015CB932200). Natural Science Funds of the Education Committee of Jiangsu Province (18KJA430009), "High-Level Talents in Six Industries" of Jiangsu Province (XYDXX-019), J.C-G acknowledges financial support from the Spanish Ministry of Economy and Competitiveness through projects MAT2014-57652-C2-1/2-R (LAPSEN) and PCIN-2015-169-C02-01/02 (MOFSENS) and through the Severo Ochoa Programme for Centers of Excellence (SEV-2016-0686) and the Campus of International Excellence (CEI) UAM+CSIC. J. C-G. and C. S. are also grateful to the China Scholarship Council (201608390023) for a PhD sponsorship.

Received: ((will be filled in by the editorial staff))
Revised: ((will be filled in by the editorial staff))
Published online: ((will be filled in by the editorial staff))

References

[1] Lipomi, D. J.; Bao, Z. *Mrs Bull.* **2017**, *42*, 93.

[2] Heo, S. W.; Lee, E. J.; Han, Y. W.; Lee, Y. S.; Lee, W. J.; Choa, S.-H.; Kim, Y. S.; Moon, D. K. *J. Ind. Eng. Chem.* **2017**, *53*, 68.

[3] Spano, F. C.; Silva, C. In *Annual Rev. Phys. Chem., Vol 65*; Johnson, M. A., Martinez, T. J., Eds. 2014; Vol. 65, p 477.

[4] Grimsdale, A. C.; Chan, K. L.; Martin, R. E.; Jokisz, P. G.; Holmes, A. B. *Chem. Rev.* **2009**, *109*, 897.

[5] Honmou, Y.; Hirata, S.; Komiyama, H.; Hiyoshi, J.; Kawauchi, S.; Iyoda, T.; Vacha, M. *Nature Commun.* **2014**, *5*, 4666

[6] Friend, R. H.; Gymer, R. W.; Holmes, A. B.; Burroughes, J. H.; Marks, R. N.; Taliani, C.; Bradley, D. D. C.; Santos, D. A. D.; Brédas, J. L.; Lögdlund, M.; Salaneck, W. R. *Nature* **1999**, *397*, 121.

[7] Heeger, A. J. *Chem. Soc. Rev.* **2010**, *39*, 2354.

[8] So, F.; Kondakov, D. *Adv. Mater.* **2010**, *22*, 3762.

[9] Lakowicz, J. R.; Masters, B. R. *Naturwissenschaften* **1991**, *78*, 456.

[10] Shin, S. H.; Park, J. S.; Park, J. W.; Kim, H. K. *Synth. Met.* **1999**, *102*, 1060.

[11] Farinola, G. M.; Ragni, R. *Chem. Soc. Rev.* **2011**, *42*, 3467.

[12] Xie, L. H.; Yin, C. R.; Lai, W. Y.; Fan, Q. L.; Huang, W. *Prog. Polym. Sci.* **2012**, *37*, 1192.

[13] Yap, B. K.; Xia, R.; Campoyquiles, M.; Stavrinou, P. N.; Bradley, D. D. *Nature Mater.* **2008**, *7*, 376.

[14] Perevedentsev, A.; Sonnefraud, Y.; Belton, C. R.; Sharma, S.; Cass, A. E.; Maier, S. A.; Kim, J. S.; Stavrinou, P. N.; Bradley, D. D. *Nature Commun.* **2015**, *6*, 5977.

[15] And, Q. P.; Yang, Y. *J. Am. Chem. Soc.* **1996**, *118*, L1673.

[16] Scherf, U.; List, E. J. W. *Adv. Mater.* **2002**, *14*, 477.

[17] And, V. N. B.; Carter, S. A.; Scott, J. C.; Klärner, G.; And, R. D. M.; Miller, D. C. *Macromolecules* **2011**, *32*, 361.

[18] Liang, J.; Qian, Y.; Xie, L. H.; Shi, N. E.; Chen, S. F.; Deng, X. Y.; Huang, W. *Acta Phys. Chim. Sin.* **2010**, *26*, 946.

[19] Sims, M.; Bradley, D. D. C.; Ariu, M.; Koeberg, M.; Asimakis, A.; Grell, M.; Lidzey, D. G. *Adv. Funct. Mater.* **2010**, *14*, 1037.

[20] Knaapila, M.; Monkman, A. P. *Adv. Mater.* **2013**, *25*, 1090.

[21] Lin, Z. Q.; Shi, N. E.; Li, Y. B.; Qiu, D.; Zhang, L.; Lin, J. Y.; Zhao, J. F.; Wang, C.; Xie, L. H.; Huang, W. *J. Phys. Chem. C* **2011**, *115*, 4418.

[22] Liu, B.; Lin, J.; Yu, M.; Li, B.; Xie, L.; Ou, C.; Liu, F.; Li, T.; Lu, D.; Huang, W. *J. Phys. Chem. C* **2017**, *121*.

[23] Lin, J.; Yu, Z.; Zhu, W.; Xing, G.; Lin, Z.; Yang, S.; Xie, L.; Niu, C.; Huang, W. *Polym. Chem.* **2013**, *4*, 477.

[24] Shaw, P. E.; Ruseckas, A.; Peet, J.; Bazan, G. C.; Samuel, I. D. W. *Adv. Funct. Mater.* **2010**, *20*, 155.

[25] Pan, C.; Sugiyasu, K.; Aimi, J.; Sato, A.; Takeuchi, M. *Angew. Chem.* **2014**, *53*, 8870.

[26] Swager, T. M. *Acc. Chem. Res.* **2008**, *41*, 1181.

[27] Pogantsch, A.; Wenzl, F. P.; List, E. J. W.; Leising, G.; Grimsdale, A. C.; Müllen, K. *Adv. Mater.* **2002**, *14*, 1061.

[28] Marsitzky, D.; Vestberg, R.; Blainey, P.; Tang, B. T.; Hawker, C. J.; Carter, K. R. *J. Am. Chem. Soc.* **2001**, *123*, 6965.

[29] Wu, Y.; Zhang, J.; Fei, Z.; Bo, Z. *J. Am. Chem. Soc.* **2008**, *130*, 7192.

[30] Scherf, U.; Müllen, K. *Die Macromol. Rapid Commun.* **1991**, *12*, 489.

[31] Swager, T. *Nature Mater.* **2002**, *1*, 151.

[32] Cacialli, F.; Wilson, J. S.; Michels, J. J.; Daniel, C.; Silva, C.; Friend, R. H.; Severin, N.; Samorì, P.; Rabe, J. P.; O'Connell, M. J. *Nature Mater.* **2002**, *1*, 160.

[33] Michael; #x; Dr, J. F.; Harry; #x; Prof, L. A. *Angew. Chem. Int. Ed.* **2007**, *46*, 1028.

[34] Cardin, D. J. *Adv. Mater.* **2002**, *14*, 553.

[35] Pan, C.; Sugiyasu, K.; Wakayama, Y.; Sato, A.; Takeuchi, M. *Angew. Chem.* **2013**, *125*, 10975.

[36] Brovelli, S.; Cacialli, F. *Small* **2010**, *6*, 2796.

[37] Pan, C.; Zhao, C.; Takeuchi, M.; Sugiyasu, K. *Chem. An Asian J.* **2015**, *10*, 1820.

[38] Brovelli, S.; Latini, G.; Frampton, M. J.; Mcdonnell, S. O.; Oddy, F. E.; Fenwick, O.; Anderson, H. L.; Cacialli, F. *Nano Lett.* **2008**, *8*, 4546.

[39] Méhes, G.; Pan, C.; Bencheikh, F.; Zhao, L.; Sugiyasu, K.; Takeuchi, M.; Ribierre, J. C.; Adachi, C. *Acs Macro Lett.* **2016**, *2016*, 781.

[40] Sasaki, T.; Mawatari, Y.; Tabata, M. *Polym. Chem.* **2015**, *6*, 8012.

[41] Wang, S.; Feng, X.; Zhang, J.; Yu, P.; Guo, Z.; Li, Z.; Wan, X. *Macromolecules* **2017**, *50*.

[42] Hoeben, F. J. M.; Jonkheijm, P.; Meijer, E. W.; Schenning, A. P. H. J. *Chem. Rev.* **2005**, *105*, 1491.

[43] Li, Y. X.; Wang, S. S.; Yu, Y.; Zhang, H.; Wang, W. Y.; Yang, R. Q.; Xie, L. H.; Liu, F.; Lin, Z. Q.; Shi, N. E. *Small* **2017**, *14*, 1703151.

[44] Liu, B.; Lin, J. Y.; Liu, F.; Yu, M. N.; Zhang, X. W.; Xia, R.; Yang, T.; Fang, Y. T.; Xie, L.; Huang, W. *Acs Appl Mater Interfaces* **2016**, *8*, 21648.

[45] Lin, J. Y.; Zhu, W. S.; Liu, F.; Xie, L. H.; Zhang, L.; Xia, R.; Xing, G. C.; Huang, W. *Macromolecules* **2015**, *47*, 1001.

[46] Bai, L. B.; Liu, B.; Han, Y. M.; Yu, M. N.; Wang, J.; Zhang, X. W.; Ou, C. J.; Lin, J. Y.; Zhu, W. S.; Xie, L. *Acs Appl Mater Interfaces* **2017**.

[47] Sasaki, T.; Yoshida, Y.; Mawatari, Y.; Tabata, M. *Macromolecules* **2015**, *48*, 889-897.

[48] Xie, L. H.; Ling, Q. D.; Hou, X. Y.; Huang, W. *J. Am. Chem. Soc.* **2008**, *130*, 2120.

[49] Moulin, E.; Niess, F.; Maaloum, M.; Buhler, E.; Nyrkova, I.; Giuseppone, N. *Angew. Chem.* **2010**, *49*, 6974.

[50] Faramarzi, V.; Niess, F.; Moulin, E.; Maaloum, M.; Dayen, J. F.; Beaufrand, J. B.; Zanettini, S.; Doudin, B.; Giuseppone, N. *Nature Chem.* **2012**, *4*, 485.

[51] Uemura, T.; Uchida, N.; Asano, A.; Saeki, A.; Shu, S.; Tsujimoto, M.; Isoda, S.; Kitagawa, S. *J. Am. Chem. Soc.* **2012**, *134*, 8360.

[52] Zheng, Y.-Q.; Yao, Z.-F.; Lei, T.; Dou, J.-H.; Yang, C.-Y.; Zou, L.; Meng, X.; Ma, W.; Wang, J.-Y.; Pei, J. *Adv. Mater.* **2017**, *29*.

[53] J. Cornil; D. A. dos Santos; X. Crispin; R. Silbey, a.; J. L. Brédas, *J. Am. Chem. Soc.* **1998**, *120*, 1289.

[54] Michels, J. J.; O'Connell, M. J.; Taylor, P. N.; Wilson, J. S.; Cacialli, F.; Anderson, H. L. *Chem. Eur-J*, **2003**, *9*, 6167.

[55] Zhang, Q.; Liu, J.; Wei, Q.; Guo, X.; Xu, Y.; Xia, R.; Xie, L.; Qian, Y.; Sun, C.; Lüer, L.; Cabanillas-Gonzalez, J.; Bradley, D. D. C.; Huang, W., *Adv. Funct. Mater.* **2018,** *28* (17), 1705824.

[56] Mróz, M. M.; Sforazzini, G.; Zhong, Y.; Wong, K. S.; Anderson, H. L.; Lanzani, G.; Cabanillas-Gonzalez, J. *Adv. Mater.* **2013**, *25*, 4347.

[57] Sun, C.; Mróz, M. M.; Castro Smirnov, J. R.; Lüer, L.; Hermida-Merino, D.; Zhao, C.; Takeuchi, M.; Sugiyasu, K.; Cabanillas-González, J., *J. Mater. Chem. C* **2018,** *6* (24), 6591.

[58] Stone, M. T.; Anderson, H. L. *Chem. Commun.* **2007**, *23*, 2387.

[59] Yau, C. M.; Pascu, S. I.; Odom, S. A.; Warren, J. E.; Klotz, E. J.; Frampton, M. J.; Williams, C. C.; Coropceanu, V.; Kuimova, M. K.; Phillips, D. *Chem. Commun.* **2008**, *25*, 2897.

[60] Frampton, M. J.; Claridge, T. D.; Latini, G.; Brovelli, S.; Cacialli, F.; Anderson, H. L. *Chem. Commun.* **2008**, *24*, 2797.

[61] Shao, S.; Hu, J.; Wang, X.; Wang, L.; Jing, X.; Wang, F. *J. Am. Chem. Soc.* **2017**, *139*, 17739.

[62] Redecker, M.; Bradley, D. D. C.; Inbasekaran, M.; Woo, E. P. *Appl. Phys. Lett.* **1998**, *73*, 1565.

[63] Sirringhaus, H.; Brown, P. J.; Friend, R. H.; Nielsen, M. M.; Bechgaard, K.; Langeveld-Voss, B. M. W.; Spiering, A. J. H.; Janssen, R. A. J.; Meijer, E. W.; Herwig; Amp, P. *Nature* 1999, *401*, 685.

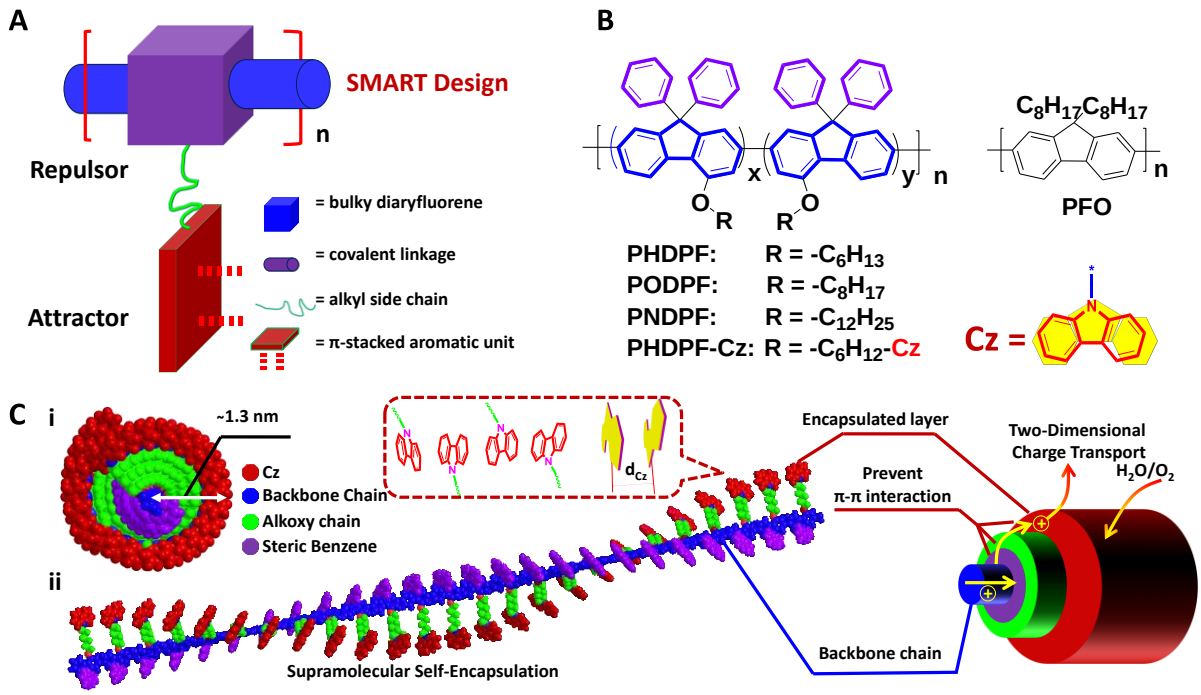

***Scheme* 1.** Schematic representation of the supramolecular self-encapsulation strategy for wide bandgap LCPs. (A) Typical molecular model of our supramolecular self-encapsulated LCPs. (B) Chemical structure of the model polymer, PHDPF-Cz, together with the controlled polyfluorenes. (C) Computer-generated model of PHDPF-Cz: i) axial and ii) lateral views. Schematic diagram illustrating the ideal molecular packing model for a PHDPF-Cz self-assembled superstructure, where the pendent Cz groups self-assemble into a sheath and act as an encapsulated layer to isolate the chain and inhibit the interchain interaction between π-π backbones, similar to previous studies.[47, 52, 53] Blue rings signify the backbone chain. Red loops indicate the Cz-threaded layers. The yellow arrow represents the 2D charge transport channel. The orange-yellow arrow denotes the penetration path for various gases, which is disrupted by the Cz-threaded layer.

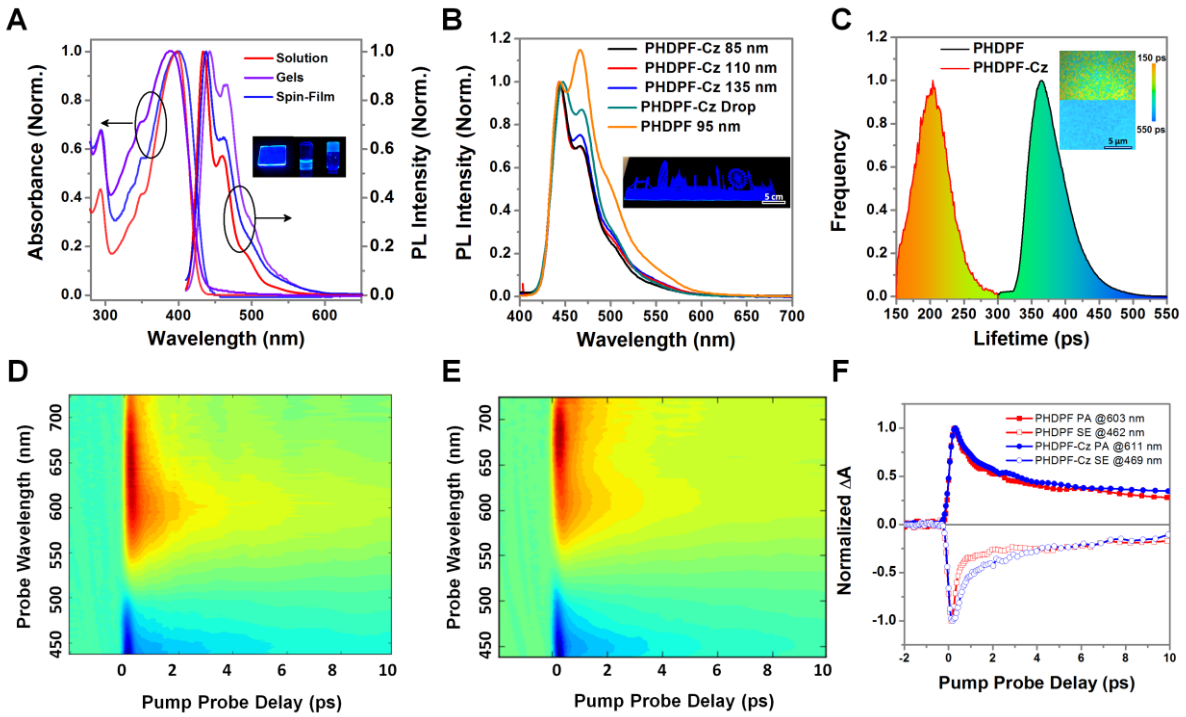

Figure 1. Optical properties of PHDPF-Cz in various states. (A) Absorbance and PL spectra of PHDPF-Cz in toluene solution (10^{-3} mg/ml), pristine film spin-coated from toluene solution (10 mg/ml, 95 nm) and gels (6 mg/ml). Inset shows photographs of the PHDPF-Cz film, concentrated solution and gel taken under a UV lamp (365 nm). The colour of the light emission from the PHDPF-Cz/toluene gel is similar to the pristine concentrated solution and corresponding spin-coated film. (B) PL spectra of PHDPF-Cz pristine films with varying thicknesses spin-coated from toluene and $CHCl_3$ solutions, together with PL spectrum of transparent film drop-coated from toluene (Drop-cast film: 2 mg/ml). Inset shows a photograph of a PHDPF-Cz film on a large-scale flexible PET substrate prepared using a scraping method from toluene solution (0.5 mg/ml; under 365 nm UV light; scale: 30 cm × 20 cm). (C) Fluorescence lifetime distribution histograms of PHDPF-Cz and PHDPF films spin-coated from toluene solution (90-100 nm). Inset shows the corresponding FLIM images. Top: PHDPF-Cz. Bottom: PHDPF. Contour plots of transient absorption spectra of (D) PHDPF and (E) PHDPF-Cz pristine spin-coated films from toluene solution. (F) ΔT/T kinetics of PHDPF and PHDPF-Cz in pristine spin-coated films upon pumping with 6.8×10^{-3} mJ/cm^2.

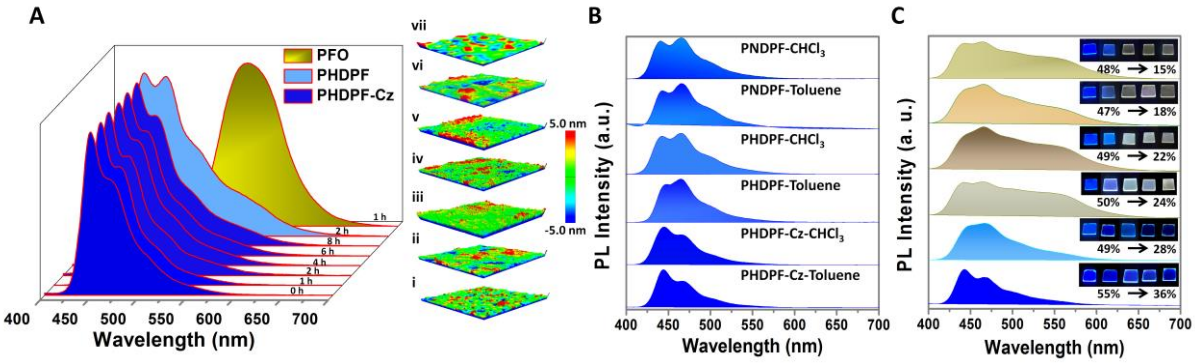

Figure 2. Ultrastable emission spectra of polyfluorene films. (A) PL spectra of the PHDPF-Cz, PHDPF and PFO spin-coated film after thermal annealing at 220 °C for varying times in ambient atmosphere. 3D AFM images of the corresponding films taken after thermal annealing for different times: (i~vi) PHDPF-Cz pristine film annealed for approximately 1 h, 2 h, 4 h, 6 h and 8 h; (vii) PHDPF film annealed for approximately 2 h. Scale bar dimensions are 6 μm × 6 μm. PL spectra of PHDPF-Cz, PHDPF and PNDPF pristine (B) and aged (C) films spin-coated from toluene (all films have a thickness of approximately 90~100 nm) and $CHCl_3$ (film thickness of 95~105 nm). Aged films were obtained by storing the pristine films in ambient atmosphere for 21 days (Humidity: 50%, Temperature: 301 K, Daylight). Insets show photographs and the PLQY of films stored under air for 0 and 21 days. PLQY of all films decreased with prolonged aging times.

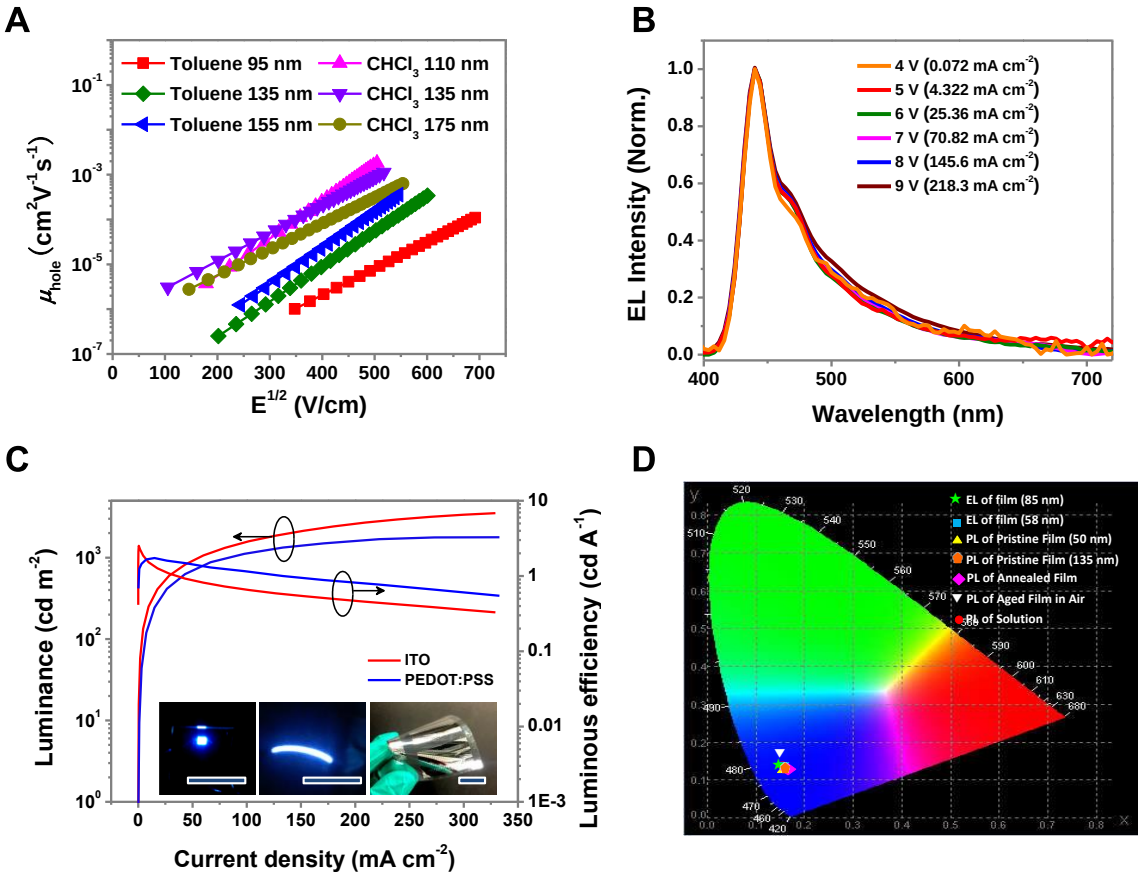

Figure 3. Electrical properties of PHDPF-Cz. (A) Hole mobility of PHDPF-Cz films with varying thicknesses. The structure for the hole-dominated device is ITO/PEDOT:PSS/PHDPF-Cz film/MoO_3/Al. The MoO_3 layer can effectively block electron injection and avoid charge (electron/hole) recombination at high current density. (B) EL spectra of PHDPF-Cz films spin-coated from toluene solution at varying voltages (film thickness is approximately 110 nm.). (C) Luminous efficiency-luminance characteristics of conventional and flexible PLEDs based on PHDPF-Cz films (110 nm). Photographs show ultrathin PHDPF-Cz solid (ITO is used as the electrode) and flexible (PEDOT:PSS blended material is used as the electrode) PLEDs driven at 25 mA cm^{-2}. Scale bar corresponds to approximately 30 mm. (D) Ultrastable PL and EL CIE for PHDPF-Cz in various solid states.

The table of contents entry should be 50−60 words long, and the first phrase should be bold. The entry should be written in the present tense and impersonal style.
Ultrastable wide-bandgap conjugated polymers are obtained via effective isolating and encapsulating chain based on supramolecular self-encapsulation mechanism, which preserves the fundamental opto-electronic property of conjugated backbone core and also improves the spectral and morphological stability. Thickness-insensitive emission behavior enable it excellent film-processing ability with a higher reproducibility. Larger-scale flexible deep-blue electroluminescent devices with a single-chain excitonic behavior are also fabricated.

Keyword: Ultrastable, Self-encapsulated strategy, Deep blue, Polyfluorene, Flexible electroluminescent devices

Jinyi Lin, Bin Liu, Mengna Yu, Xuhua Wang, Zongqiong Lin, Xinwen Zhang, Chen Sun, Juan Cabanillas-Gonzalez, Linghai Xie*, Feng Liu, Changjin Ou, Lubing Bai, Yamin Han, Man Xu, Wensai Zhu, Trevor A. Smith, Paul N. Stavrinou, Donal D. C. Bradley* and Wei Huang*

Ultrastable Supramolecular Self-encapsulated Wide-bandgap Conjugated Polymers for Large-area and Flexible Electroluminescent Devices

ToC figure ((Please choose one size: 55 mm broad × 50 mm high **or** 110 mm broad × 20 mm high. Please do not use any other dimensions))

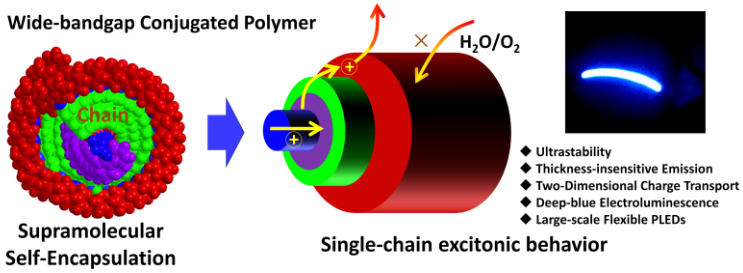

Supporting Information

Ultrastable Supramolecular Self-encapsulated Wide-bandgap Conjugated Polymers for Large-area and Flexible Electroluminescent Devices

Jinyi Lin, Bin Liu, Mengna Yu, Xuhua Wang, Zongqiong Lin, Xinwen Zhang, Chen Sun, Juan Cabanillas-Gonzalez, Linghai Xie, Feng Liu, Changjin Ou, Lubing Bai, Yamin Han, Man Xu, Wensai Zhu, Trevor A. Smith, Paul N. Stavrinou, Donal D. C. Bradley* and Wei Huang**

((Optional Dedication))

Professor Dr Wei Huang, Professor Dr Feng Liu, Dr Jinyi Lin, Dr Changjin Ou, Mr Lubing Bai, Miss Yamin Han, Miss Man Xu, Mr Wensai Zhu
Key Laboratory of Flexible Electronics (KLOFE) & Institute of Advanced Materials (IAM), Jiangsu National Synergetic Innovation Center for Advanced Materials (SICAM), Nanjing Tech University (NanjingTech), 30 South Puzhu Road, Nanjing 211816, China.
E-mail: wei-huang@njtech.edu.cn
Professor Dr Donal D.C. Bradley, Dr Jinyi Lin
Departments of Engineering Science and Physics and Division of Mathematical, Physical and Life Sciences, University of Oxford, 9 Parks Road, Oxford OX1 3PD, UK.
Email: donal.bradley@mpls.ox.ac.uk
Professor Dr Donal D.C. Bradley, Professr Dr Paul N. Stavrinou, Dr Xuhua Wang, Dr Jinyi Lin
Department of Physics and Centre for Plastic Electronics, The Blackett Laboratory, Imperial College London, Prince Consort Road, London SW7 2AZ, UK.
Professor Dr Wei Huang, Professor Dr Linghai Xie, Professor Dr Xinwen Zhang, Dr Bin Liu, Miss Mengna Yu
Center for Molecular Systems and Organic Devices (CMSOD), Key Laboratory for Organic Electronics and Information Displays & Institute of Advanced Materials (IAM), Jiangsu National Synergetic Innovation Center for Advanced Materials (SICAM), Nanjing University of Posts & Telecommunications, 9 Wenyuan Road, Nanjing 210023, China.
E-mail: iamlhxie@njupt.edu.cn
Professor Dr Juan Cabanillas-Gonzalez, Miss Chen Sun
Madrid Institute for Advanced Studies (IMDEA Nanociencia), Ciudad Universitaria de Cantoblanco, Calle Faraday 9, Madrid 28049, Spain.
Professor Dr Trevor A. Smith, Miss Mengna Yu,
ARC Centre of Excellence in Exciton Science, School of Chemistry, The University of Melbourne, Parkville VIC 3010, Australia.
Professor Dr Paul N. Stavrinou
Department of Engineering Science, University of Oxford, Parks Road, Oxford OX1 3PD, UK.
Professor Dr Wei Huang, Professor Dr Zongqiong Lin, Dr Jinyi Lin,
Shaanxi Institute of Flexible Electronics (SIFE), Northwestern Polytechnical University (NPU), 127 West Youyi Road, Xi'an 710072, Shaanxi, China.
Keywords: Ultrastable, Self-encapsulated strategy, Deep blue, Polyfluorene, Flexible electroluminescent devices

Supplementary Materials

- Scheme S1**.** Synthetic routes of PHDPF-Cz.
- Figure S1. ^{1}H and ^{13}C spectra of monomer and polymer.
- Figure S2. GPC curves of PFO, PHDPF, PODPF, PNDPF and PHDPF-Cz.
- Figure S3. TGA curve of PHDPF-Cz.
- Figure S4. DSC curve of PHDPF-Cz.
- Figure S5. CV curve of PHDPF-Cz.
- Figure S6. Axial (Left) views of DBrHDPF-Cz in a crystallized form. Molecular packing mode of DBrHDPF-Cz single crystal.
- Figure S7. PL spectra of DBrHDPF-Cz for diluted solution and a single crystal. The PL spectrum of the single crystal was measured by using front-face detection to minimize the effect of self-absorbance. The inset shows photographs of the DBrHDPF-Cz diluted solution and single crystal under UV light (345 nm). The single crystal size is approximately 2 mm × 0.5 mm × 0.2 mm.
- Figure S8. Photographs of polyfluorenes in concentrated toluene solutions (6 mg/ml) after ageing for 30 min at room temperature, including PHDPF-Cz (Cz), PHDPF (C6), PODPF (C8), PNDPF (C12) and PFO.
- Figure S9. CD spectra of PHDPF-Cz in various states together with the PHDPF film drop-coated from toluene solution as comparison.
- Figure S10. Out of plane (OOP, Left) and in plane (IP, Right) X-ray scattering profiles of various spin-coated films on Si substrates.
- Figure S11**.** Grazing incidence X-ray scattering (GIXD) images of PHDPF-Cz (A) and PHDPF (B) films spin-coated from toluene solution.
- Figure S12**.** A possible model developed on the basis of the GIXD data shows that the grooves are derived from the PHDPF-Cz chain in the spin-coated films. “d” represents the interchain backbone distance in PHDPF-Cz films. “dCz” is the standard π-stacking distance among interchain or intrachain pendent Cz units. The inset also shows an AFM image of the PHDPF-Cz film spin-coated from toluene solution.
- Figure S13. AFM (a) and Grazing-incidence-X-ray scattering (GIXD) (b) images of PHDPF-Cz films spin-coated from $CHCl_3$ solution with the concentration of 10 mg/ml.
- Figure S14**.** AFM and Grazing-incidence-X-ray scattering (GIXD) images of PHDPF films spin-coated from toluene (a, b) and $CHCl_3$ (c, d) solution with the concentration of 10 mg/ml, together with their AFM images, respectively.
- Figure S15. AFM and Grazing-incidence-X-ray scattering (GIXD) images of PNDPF

films spin-coated from toluene (a, b) and $CHCl_3$ (c, d) solution with the concentration of 10 mg/ml, together with their AFM images, respectively.

- Figure S16**.** PL decays of the PHDPF-Cz in toluene solution (top) and gels (bottom) at different wavelengths. 2D Time-resolved PL spectra are shown in the inset.
- Figure S17**.** PL spectra of PHDPF (Top) and PNDPF (Bottom) films spin-coated from toluene and $CHCl_3$ solutions with the different thickness.
- Figure S18**.** Absorbance spectra of PHDPF-Cz and PHDPF films spin-coated from toluene solutions with the different thickness.
- Figure S19**.** Absorbance and PL spectra of PHDPF-Cz films spin-coating from $CHCl_3$ solution after thermal annealing at 200 °C in N_2 (Top) and in air (Bottom) for 0, 3 and 6 hours. Thickness is about 80 nm.
- Figure S20**.** PL spectra of PHDPF-Cz, PHDPF and PFO aged films (all about 90~100 nm) and $CHCl_3$ (all about 95~105 nm). PL spectra of PHDPF-Cz, PHDPF and PFO films spin-coated from toluene with various times under UV lamp in ambient atmosphere (Humidity: 50%, Temperature: 301 K, Daylight.). Insets show the photographs of films keeping under air at 16 h.
- Figure S21**.** PL spectra of PFO films spin-coated from 1,2-dichloroethane (DCE) (β Phase film, 88 nm), toluene (Amprohous film with lower content of β phase, 85 nm) and $CHCl_3$ (amorphous film, 80 nm) solutions under aging 3 days under the air and daylight.
- Figure S22**.** PL spectra of PHDPF-Cz, PHDPF (PC6) and PNDPF (PC12) films spin-coated from toluene and $CHCl_3$ solutions under aging 21 days in the N_2 atmosphere.
- Figure S23**.** EL spectra of PLEDs based on PHDPF-Cz film spin-coating from toluene solution with the concentration of 6 mg/ml (58 nm).
- Figure S24**.** EL spectra of PLEDs based on PHDPF-Cz film spin-coating from $CHCl_3$ solution with the concentration of 10 mg/ml (100 nm).
- Figure S25**.** EL spectra of PLEDs based on PHDPF-Cz film spin-coated from $CHCl_3$ solution with the concentration of 6 mg/ml (63 nm).
- Figure S26**.** Current-density-brightness-luminous-efficiency characteristics of PLEDs based on PHDPF-Cz films spin-coated from toluene (95 nm) and $CHCl_3$ (100 nm).
- Figure S27**.** Current-density-brightness-luminous-efficiency characteristics of PLEDs based on PHDPF-Cz films spin-coated from toluene (58 nm) and $CHCl_3$ (63 nm).
- Figure S28**.** EL spectra of PLEDs based on PHDPF film spin-coating from toluene solution with the concentration of 10 mg/ml (92 nm), similar to PNDPF under the same experimental conditions.

- Figure S29**.** EL spectra of PLEDs based on PHDPF film spin-coated from toluene solution with the concentration of 6 mg/ml (58 nm), similar to PNDPF under the same experimental conditions.
- Figure S30**.** Current-density-brightness-luminous-efficiency characteristics of PLEDs based on PHDPF films spin-coated from toluene with the concentration of 10 mg/ml and 6 mg/ml.
- Table S1**.** The fitting results of PL decay curves as single or double exponential decay functions.

EXPERIMENTAL SECTION

Chemicals

All reagents were purchased from Sigma-Aldrich, Merck and Alfa Aesar, and used as received unless stated otherwise. Anhydrous THF (HPLC grade) was collected from Solvent Purification Systems (Innovative Technology, Inc.). Anhydrous chloroform was pre-dried over molecular sieves.

Characterization

^{1}H- and ^{13}C-NMR spectrum was recorded on a Bruker 400 MHz spectrometer in $CDCl_3$ with tetramethylsilane (TMS) as the interval standard. Mass spectra were recorded on a Shimadzu GCMS 2010 PLUS. Gel permeation chromatography (GPC) analysis was performed on a HP1100 HPLC system equipped with 7911GP-502 and GP NXC columns using polystyrenes as the standard and tetrahydrofuran (THF) as an eluent at a flow rate of 1.0 mL/min at 25 ^{o}C. Absorption spectra were measured with a Shimadzu UV-3600 spectrometer at 25 ^{o}C, and emission spectra were recorded on a Shimadzu RF-5301(PC) luminescence spectrometer. DSC measurement was acquired using a Shimadzu Instruments DSC-60A. DSC data were collected from 30 to 245 ^{o}C at a rate of 10 ^{o}C/min for both of the baseline and sample. Thermogravimetric analyses (TGA) were conducted by a Shimadzu DTG-60H under a heating rate of 10 ^{o}C/min and a nitrogen flow rate of 50 cm^3/min. Cyclic voltammetric (CV) studies were conducted using an CHI660C Electrochemical Work station in a typical three-electrode cell with a platinum sheet working electrode, a platinum wire counter electrode, and a silver/silver nitrate (Ag/Ag^+) reference electrode. All electrochemical experiments were carried out under a nitrogen atmosphere at room temperature in an electrolyte solution of 0.1 M tetrabutylammonium hexafluorophosphate (n-Bu_4NPF_6) in CH_2Cl_2 at a sweeping rate of 0.1 V/s. According to the redox onset potentials of the CV measurements, the HOMO/LUMO energy levels of the materials are estimated based on the reference energy level of ferrocene (4.8 eV below the vacuum): HOMO/ LUMO = -[E_{onset} –$E_{(Fc/Fc+)}$+ 4.8] eV. For scanning

electron microscopic (SEM) studies, a drop of 20 μL solutions were placed onto silicon substrates, and the solvent was left to evaporate. The samples were then examined with a field emission SEM (Hitachi, S-4800) at an accelerating voltage of 3 kV. The film morphologies of polymer films were recorded with a Bruker's Dimension Icon AFM in tapping mode (Bruker's Sb/Si probe tipwith a resonant frequency 320 kHz and the spring constant 42 Nm^{-1}). The corresponding film thicknesses were measured using a Bruker Dektak XT stylus profiler. The monomer single crystal data collection was performed at 100 or 298 K on a Bruker 2000 CCD area detector using graphite-monochromated Mo Kα radiation (λ = 0.71073 Å). All structures were solved by direct methods using OLEX2 and refined against F^2 using SHELXL-2014. Hydrogen atoms were fixed geometrically and refined isotropically. To measure the fluorescence lifetime, the incident 390 nm, 150-fs laser pulses were generated from a Coherent TOPAS-C optical parametric amplifier; pumped by a 1 kHz Coherent Legend regenerative amplifier that is seeded by a Coherent Vitesse oscillator. These input laser pulses were focused by a lens (f = 20 cm) on the samples solution in a 1-mm-thick quartz cell (beam spot ~1 mm inside the cell). The emission from the samples was collected at a backscattering angle of 150° by a pair of lenses and directed to an Optronis Optoscope™ streak camera system which has an ultimate temporal resolution of 6 ps. CD spectra were collected using a JASCO J-820 spectropolarimeter (Tokyo, Japan) and CD measurements were from 300 to 450 nm, the data pitch was 0.5 nm, scan speed was 800 nm/min, response time was 0.5 s, and bandwidth was 1 nm. GIXD measurements were performed on Beamline 7.3.3 at the Advanced Light Source (ALS) at the Lawrence Berkeley National Laboratory. An X-ray beam impinged onto the sample at a grazing angle above and below the critical angle of the polymer film (αc = 0.16), but below the critical angle of the silicon substrate (αc = 0.22). The wavelength of X-rays was 1.240 Å, and the scattered intensity was detected by PILATUS 1M detector. The sample was loaded on silicon nitride substrate, and the beam energy used here is 284.4 eV which generally probes the carbon edge resonance. The thicknesses of

polymer films were measured using a Bruker 129 Dektak XT stylus profiler. A Becker & Hickl SPC-830 FLIM module coupled to a modified Olympus confocal scanning microscope (FV300/IX71) was employed for the time-resolved fluorescence imaging measurements.

Preparation of DBrHDPF-Cz single crystals:

Firstly, DBrHDPF-Cz (2 mg) was dissolved in dichloromethane (2 ml) at room temperature. Then, ethanol (0.5 ml) was added into DBrHDPF-Cz solution on the interface. After several days, we can obtain the DBrHDPF-Cz single crystal.

Preparation of polymer solution, gels and films:

The preparation of polymer solutions were carried out by dissolving the polymer in the organic solvents spontaneously overnight. Various concentrated polymers solution for spin-coating process are obtained after the heated solutin cool to room temperature. Espeial for PHDPF-Cz, the precursor concentrated solution must be aged several minutes (about 5 min.) to allow for gelation processing induce π-π stacked interaction of Cz and further form MWs for fabricating spin-coated films. Beacause the π-π stacked interaction of Cz in the solid states play a key role to induce the formation PHDPF-Cz MWs.

PHDPF-Cz gels were prepared by agitating their solutions at 100 ˚C for 10 min, where a macroscopically homogeneous solution was obtained once fully dissolved. The PHDPF-Cz-based gels were prepared by aging the solutions with different concentrations at room temperature. In analyzing the critical concentration of gels in various solvents, 5 mg of PHDPF-Cz and 50 μL of solvents were successively added into a sealed glass via diluting the solution concentration threshold of a gel formation.

Pristine films of polymers for UV-*vis* and PL spectra, GIXD analysis, photostable experiments, and themal annealing were spin-casted on quartz (For optical analysis) or silican (For GIXD analysis) substrates from their toluene or chloroform solution (various concentration) using KW-4A (from the institute of micro-electronics of Chinese Academy of Science) at 1500 rpm for 30 s. After the films were cooled to the ambient temperature, UV-*vis*

absorption and PL spectra of polymers were measured. PHDPF-Cz film for CD analysis is obtained from drop-coating from toluene solution (3 mg/ml) after thermal annealing at 50 ºC in traditional vacuum drying oven.

Mobility Measurements. The hole-only device for hole-mobility measurements consists of indium-doped tin oxide (ITO)/poly(3,4-ethylenedioxythiophene):polystyrene sulfonate (PEDOT:PSS)/PHDPF-Cz/MoO_3/Al. The PHDPF-Cz films were obtained via spin-coating from toluene and $CHCl_3$ solution. Film thicknesses were controlled via changing the solution concentrations. The pre-etched ITO substrate was treated with UV/ozone for 30 min, and then a 40 nm PEDOT:PSS layer was spin-coated onto the ITO substrate from an aqueous solution, followed by baking in an oven at 150 ºC for 20 min. The solution of PHDPF-Cz was spin-coated on the PEDOT:PSS layer to yield the film. A bi-layer cathode structure of MoO_3 (20 nm)/Al (100 nm) was thermally evaporated on top of the HTM layer. J-V characteristics of the devices were measured with a Keithley 2400 Source-Measure unit interfaced with a computer.

Device Fabrication: The structure of devices is ITO/PEDOT:PSS (PEDOT:PSS blended materials as electrode)/polymers film /TPBI/Al (80 nm). Polymer films were spin-coated from their toluene and $CHCl_3$ solution with various thicknesses. The background pressure of the chamber was under 10^{-6} Torr during the deposition process. The layer thickness of the deposited material was monitored in situ using an oscillating quartz thickness monitor. The EL spectra and Commission Internationale de L'Eclairage (CIE) coordination of the devices were measured using a PR650 Spectroscan spectrometer.

Supplementary Materials

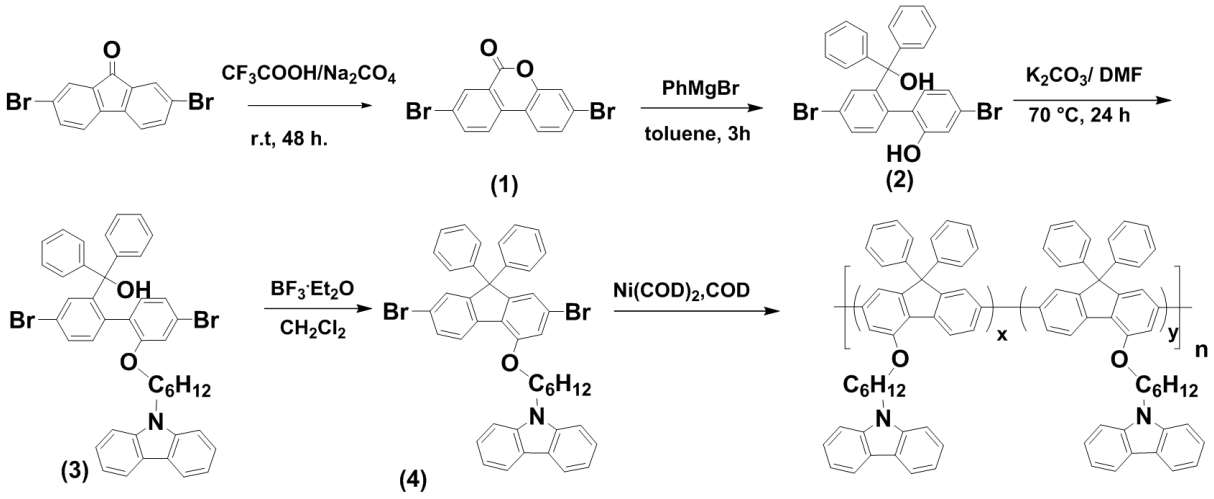

***Scheme* S1.** Synthetic routes of PHDPF-Cz.

(2'-(6-(9H-carbazol-9-yl)hexyloxy)-4,4'-dibromobiphenyl-2-yl)diphenylmethanol (3). To a solution of K_2CO_3 (0.97 g, 7 mmol) and **(2)** (1.02 g, 2 mmol) in DMF (3 mL) was added dropwise 9-(6-bromohexyl)-9H-carbazole (0.79 g, 2.4 mmol). The mixture was heated to 70 ^oC for 24 hours in the dark under the nitrogen. After the solids were filtered off, the mother liquor was treated with 1 M HCl and petroleum ether. The water phase was extracted three more times with dichloromethane, and the combined extract was washed three times with 1 M HCl, then with water for three times. The mixture solution was dried with anhydrous $MgSO_4$. The solvents were removed by rotary evaporation, and the crude product was purified by column chromatography using petroleum ether: dichloromethane=3:1 as eluent to provide a white solid (1.063 g, yield 70%). MALDI-TOF-MS (*m/z*): 759.44 (M^+). ^1H NMR (400 MHz, $CDCl_3$, ppm): 8.124-8.115 (d, 2H, Ar H), 7.495-7.457 (t, 2H, Ar H), 7.415-7.366 (m, 3H, Ar H), 7.281-7.232 (m, H, Ar H), 7,185-7.169 (m, 3H, Ar H), 7.103-7.069 (m, 3H, Ar H), 6.881-6.877 (d, 1H, Ar H), 6.833-6.813 (d, 1H, Ar H), 6.697-6.673 (dd, 1H, Ar H), 6.159-6.139 (d, 1H, Ar H), 4.320-4.285 (t, 2H, CH_2 H), 3.953 (s, 1H, OH H), 3.901-3.753 (m, 2H, OCH_2 H), 1.919-1.807 (m, 2H, CH_2 H), 1.637-1.583 (m, 2H, CH_2 H), 1.338-1.286 (m, 4H, CH_2 H). ^{13}C NMR (125 MHz, $CDCl_3$, ppm): δ 155.629, 148.196, 146.379, 145.860, 140.405, 135.835, 134.211, 132.804, 132.139, 130.239, 129.605, 128.061, 127.842, 127.601, 127.305, 126.893,

125.624, 123.097, 122.832, 121.749, 121.137, 120.357, 118.770, 115.150, 108.632, 82.050, 68.655, 53.416, 42.810, 31.592, 28.895, 28.676, 26.782, 25.656, 22.657, 14.118.

9-(6-(2,7-dibromo-9,9-diphenyl-9H-fluoren-4-yloxy)hexyl)-9H-carbazole(4) A solution of boron trifluoride–diethyl ether complex (0.15 mL) in appropriate dichloromethane (5 mL) was added dropwise to a solution of **(3)** 0.759 g (1 mmol) in appropriate dichloromethane (5 mL). The reaction mixture was stirred at r.t. (25 ^{o}C) for 24 hours. Ethanol (50 mL) and water (50 mL) was successively added to quench the reaction. And then the phases were separated and the aqueous phase was extracted with dichloromethane. The combined dichloromethane layers were washed and dried ($MgSO_4$). After removal of the solvent, the remaining crude product was purified by column chromatography using petroleum ether: dichloromethane=3:1 as eluent to provide white products. (1.027 g, yield 99%). MALDI-TOF-MS (*m/z*): 741.24 (M^+). ^{1}H NMR (400 MHz, $CDCl_3$, ppm): 8.150-8.130 (d,2H, Ar H), 7.918-7.897 (d, 1H, Ar H), 7.512-7.420 (m, 6H, Ar H), 7.281-7.239 (m, H, Ar H), 7,163-7.139 (m, 4H, Ar H), 7.116-7.112 (d, 1H, Ar H), 6.963-6.959 (d, 1H, Ar H), 4.395-4.360 (t, 2H, CH_2 H), 4.092-4.060 (t, 2H, OCH_2 H), 2.024-1.891 (m, 4H, CH_2 H), 1.658-1.490 (m, 2H CH_2 H), 1.341-1.225 (m, 2H CH_2 H). ^{13}C NMR (125 MHz, $CDCl_3$, ppm): δ 155.423, 154.083, 152.427, 144.472, 140.411, 137.606, 130.834, 128.765, 128.490, 128.067, 127.108, 125.653, 125.155, 122.850, 122.088, 121.435, 120.886, 120.415, 118.825, 113.872, 108.605, 68.302, 65.892, 42.919, 31.946, 30.954, 29.751, 29.719, 29.678, 29.383, 29.055, 29.006, 27.040, 6.070, 22.714, 14.145.

Poly[4-(6-(9H-carbazol-9-yl)hexyloxy)-9,9-diphenylfluorene]-*co*-[5-(6-(9H-carbazol-9-yl)hexyloxy)-9,9-diphenylfluorene] (PHDPF-Cz) 4 0.37 g (0.5 mmol) was added to a appropriate DMF (10 mL) and toluene (10 ml) solution containing $Ni(COD)_2$ 0.33 g (2.4 equiv) 1,5-cyclooctadiene 0.15 mL (2.4 equiv), and bpy 0.186 g (2.4 equiv) in a 50 mL Schlenk tube under argon. The reaction mixture was stirred for 36 h at 90 °C to obtain a dark blue solution. The bromobenzene was added to solution for terminating reaction. After the mixture had cooled to room temperature, 10ml THF and 1.0 ml hytrazine hydrate of was

added for quenching activator. The precipitate was separated by filtration. The solution should further purification to be subjected to alumina (Al_2O_3) column chromatography eluting with THF to afford PHDPF-Cz as a green-yellow powder (262 mg, 90%). (GPC: M_n 2.96 × 10^4, M_w 4.59 × 10^4, PDI 1.55. ^{1}H NMR (400 MHz, $CDCl_3$, ppm): 8.12-8.10 (3H, Ar H), 7.55-7.44 (6H, Ar H), 7.28-7.11 (13H, Ar H), 6.96-6.94 (1H, Ar H), 4,38-4.35 (2H, CH_2 H), 4.15-4.14 (2H, CH_2 H), 2.00-1.95 (4H, CH_2 H), 1.67-1.55 (4H, CH_2 H).

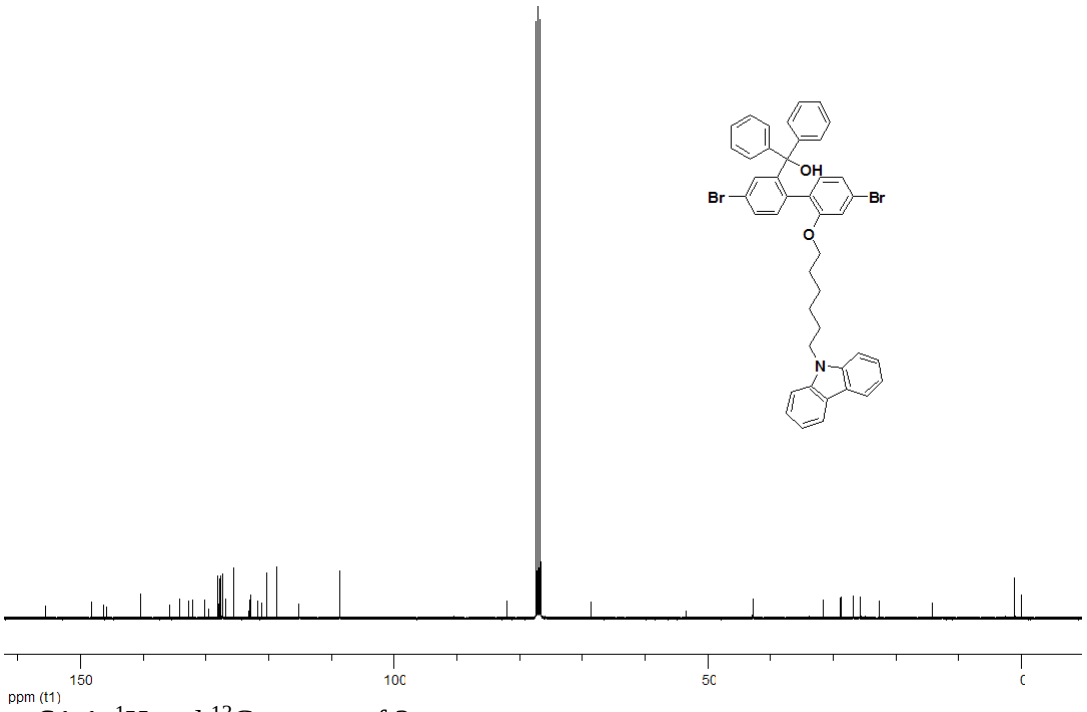

Figure S1-1. ^{1}H and ^{13}C spectra of 3

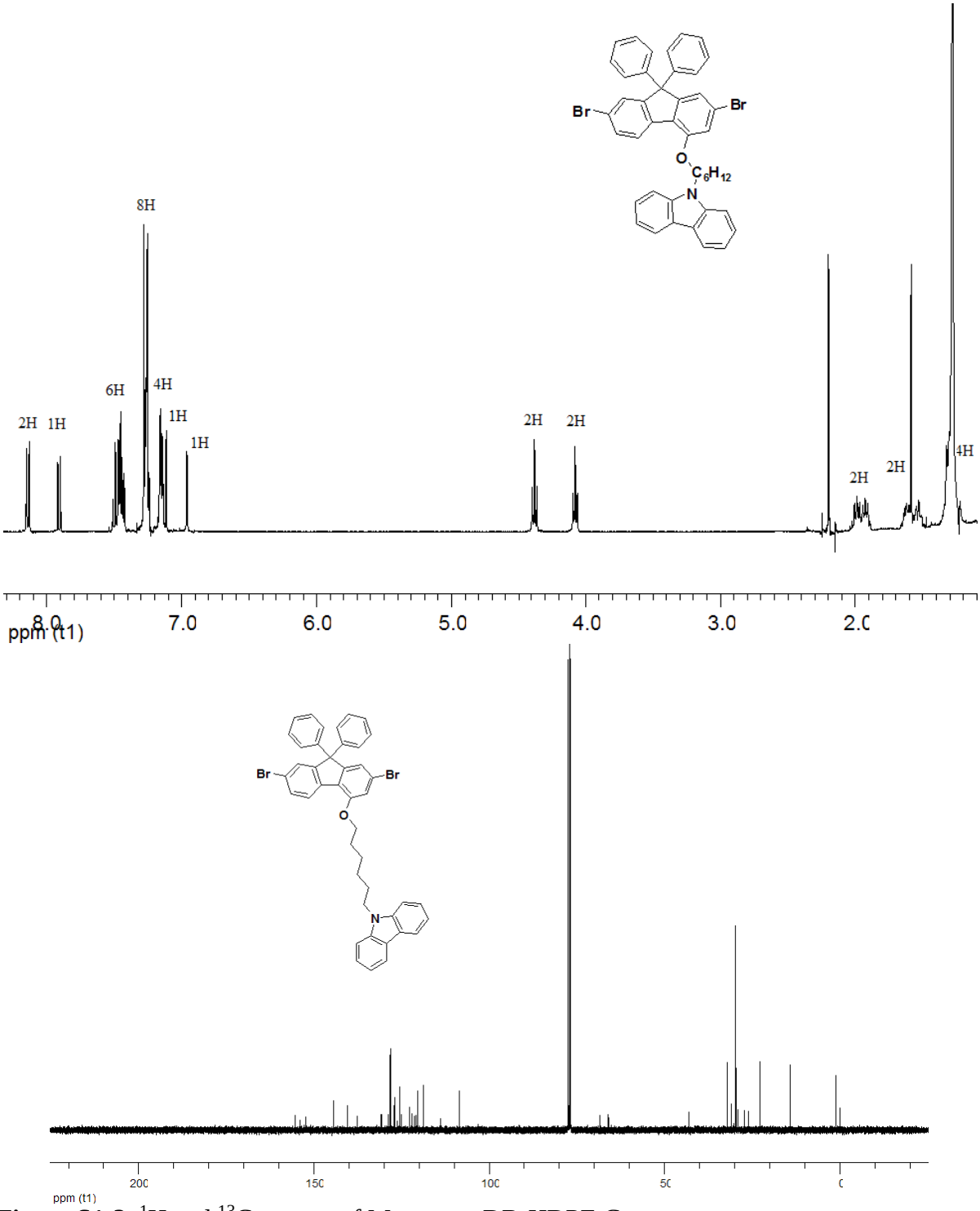

Figure S1-2. ^{1}H and ^{13}C spectra of Monomer, DBrHDPF-Cz.

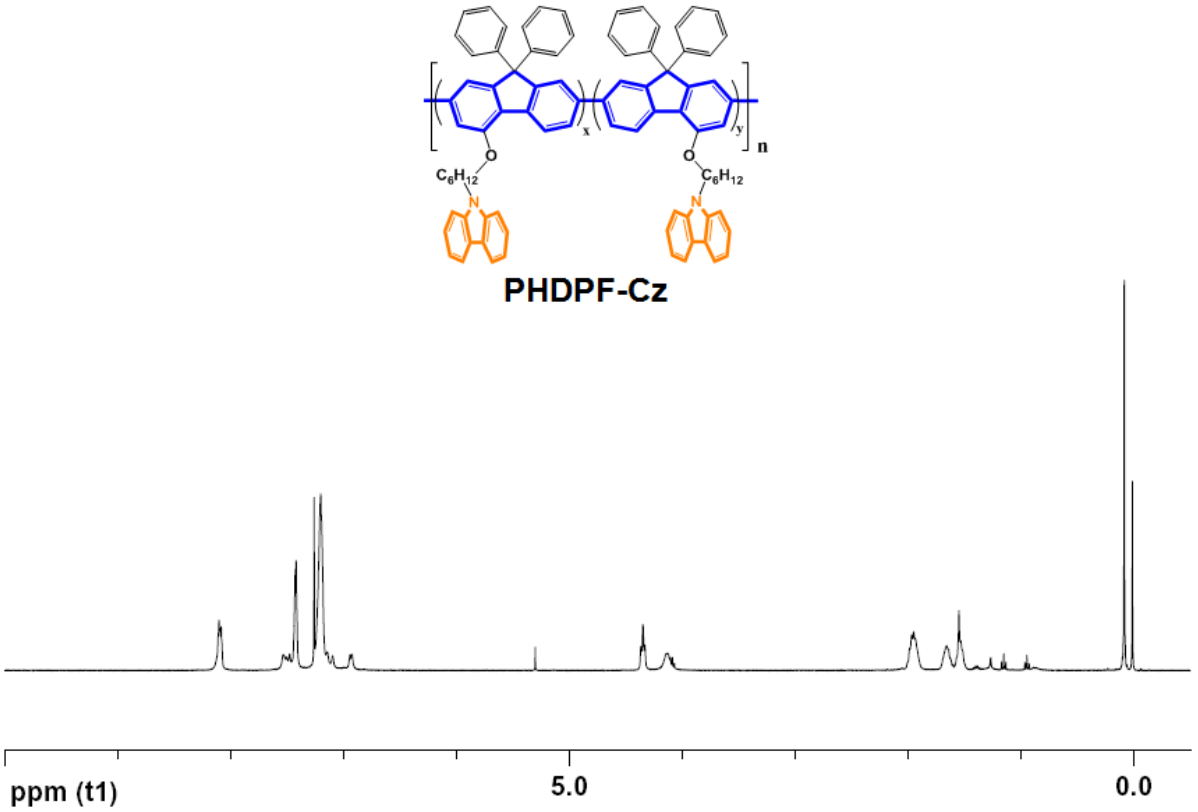

Figure S1-3. ^{1}H spectra of PHDPF-Cz.

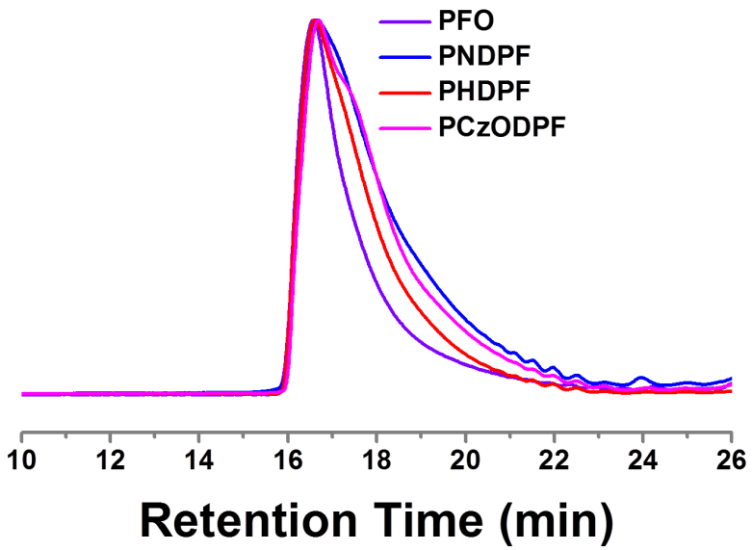

Figure S2. GPC curves of PFO, PHDPF, PODPF, PNDPF and PHDPF-Cz.

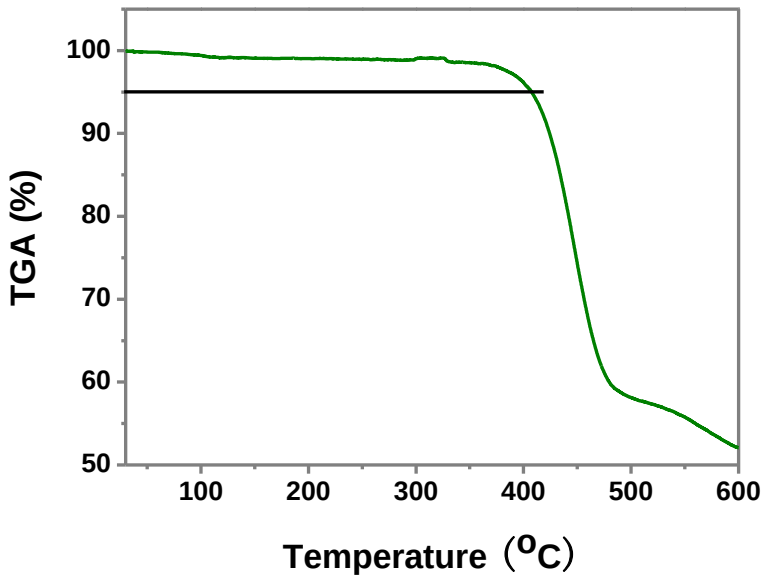

Figure S3. TGA curve of PHDPF-Cz.

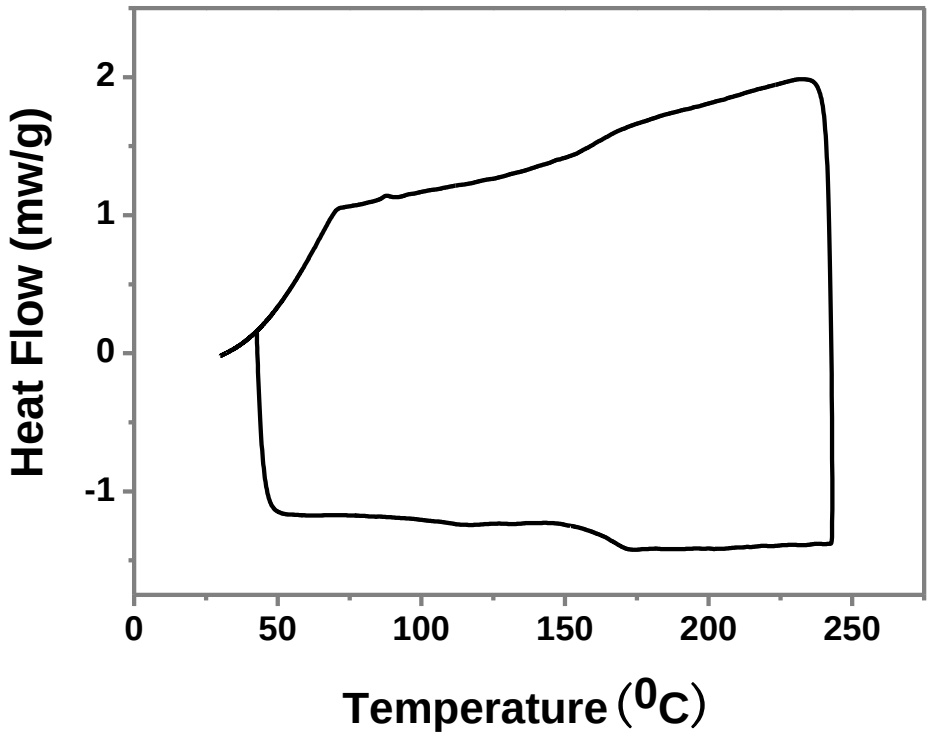

Figure S4. DSC curve of PHDPF-Cz.

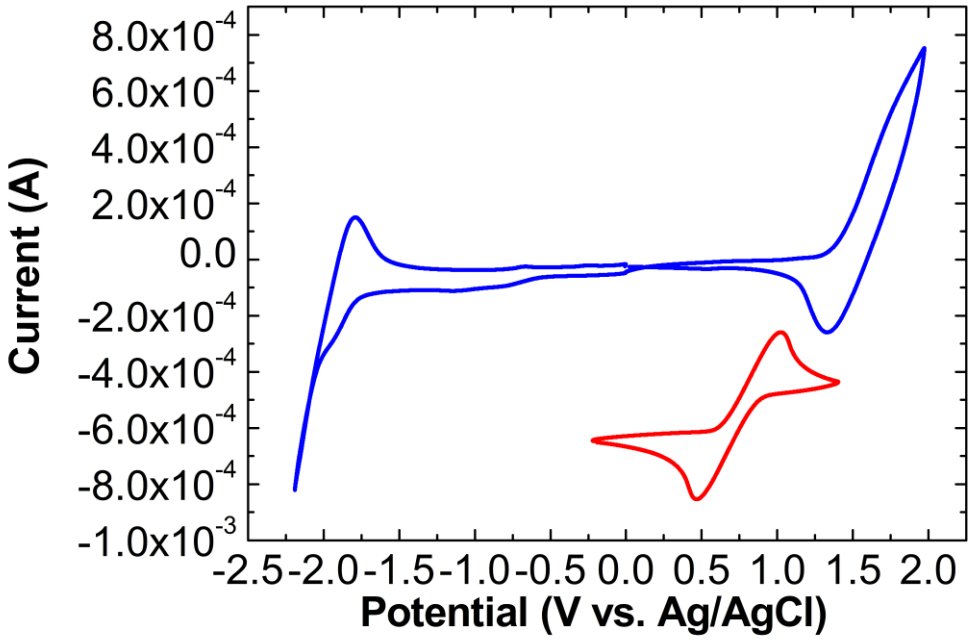

Figure S5. CV curve of PHDPF-Cz.

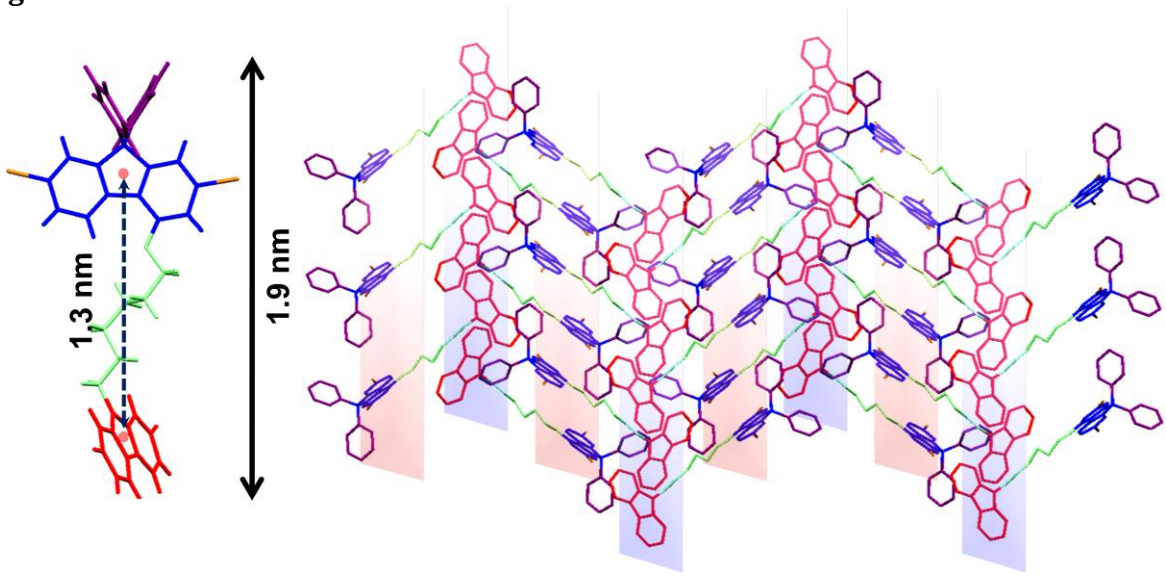

Figure S6. Axial (Left) views of DBrHDPF-Cz in a crystallized form. Molecular packing mode of DBrHDPF-Cz single crystal..

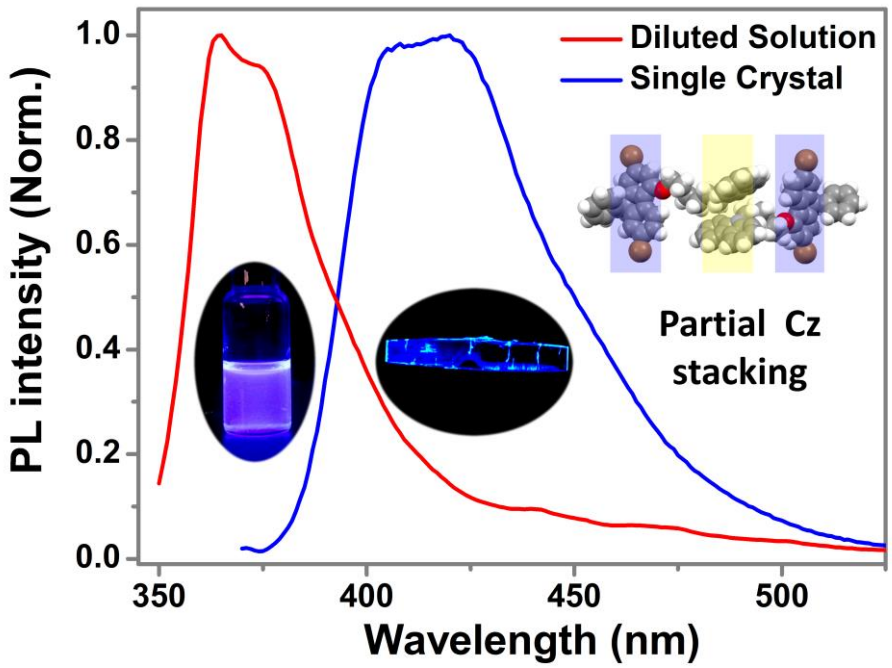

Figure S7. PL spectra of DBrHDPF-Cz for diluted solution and a single crystal. The PL spectrum of the single crystal was measured by using front-face detection to minimize the effect of self-absorbance. The inset shows photographs of the DBrHDPF-Cz diluted solution and single crystal under UV light (345 nm). The single crystal size is approximately 2 mm × 0.5 mm × 0.2 mm.

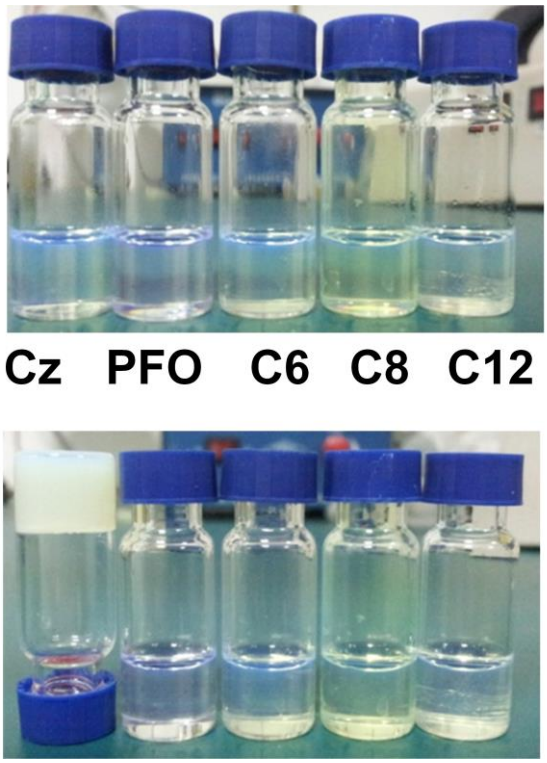

Figure S8. Photographs of polyfluorenes in concentrated toluene solutions (6 mg/ml) after ageing for 30 min at room temperature, including PHDPF-Cz (Cz), PHDPF (C6), PODPF (C8), PNDPF (C12) and PFO.

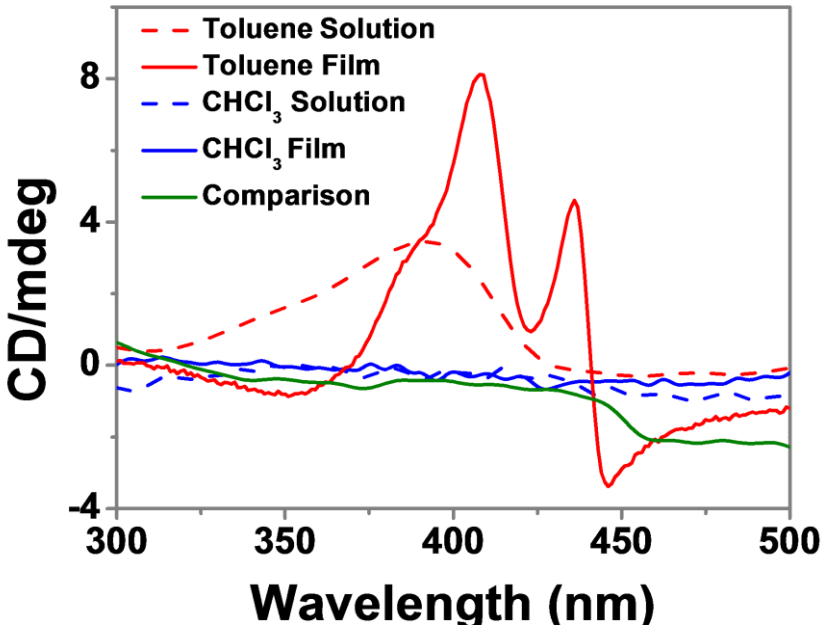

Figure S9. CD spectra of PHDPF-Cz in various states together with the PHDPF film drop-coated from toluene solution as comparison.

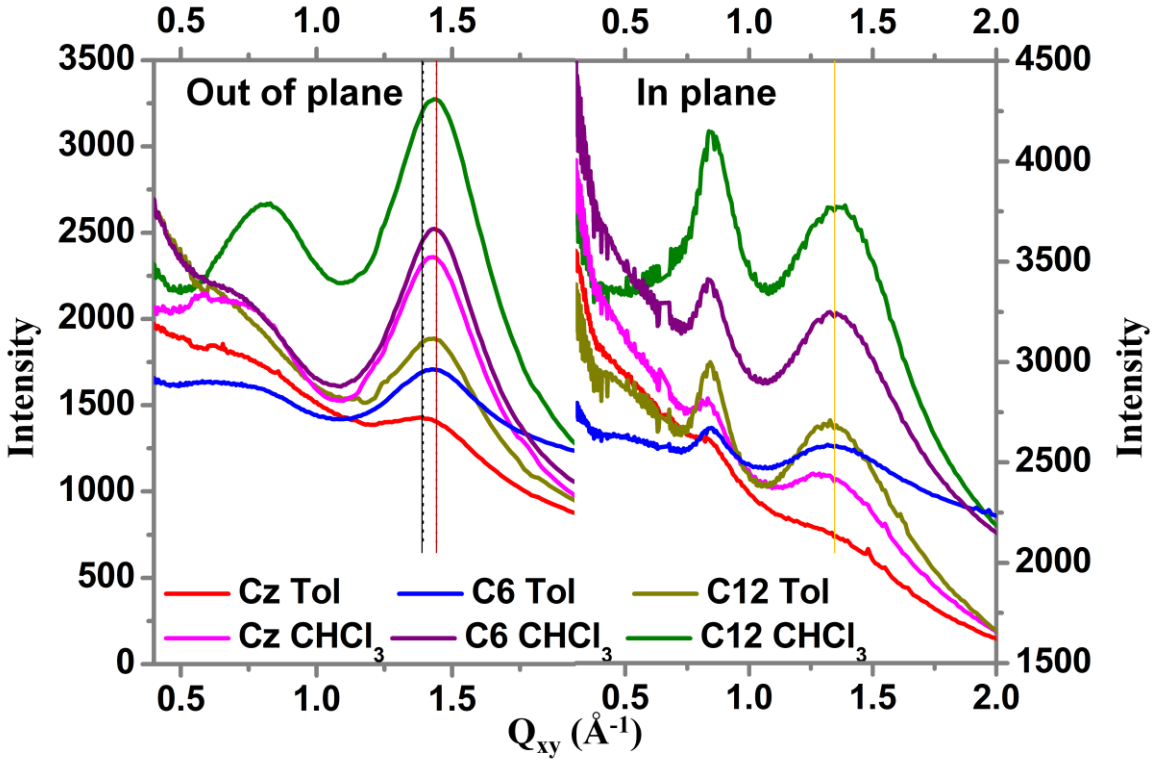

Figure S10. Out of plane (OOP, Left) and in plane (IP, Right) X-ray scattering profiles of various spin-coated films on Si substrates.

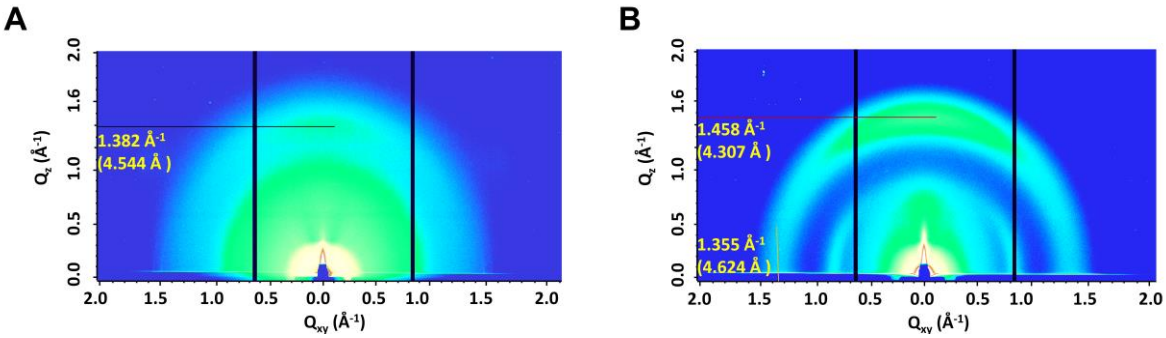

Figure S11. Grazing incidence X-ray scattering (GIXD) images of PHDPF-Cz (A) and PHDPF (B) films spin-coated from toluene solution.

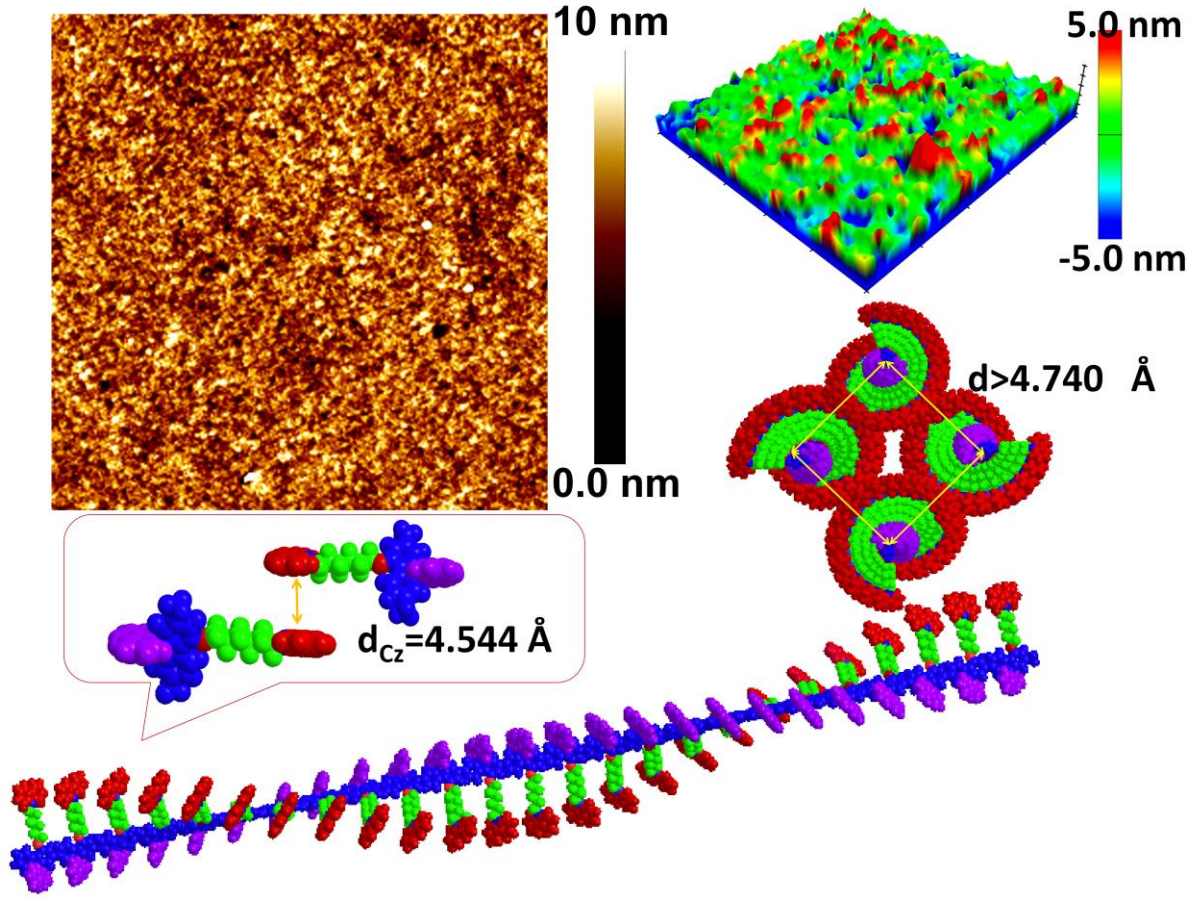

Figure S12. A possible model developed on the basis of the GIXD data shows that the grooves are derived from the PHDPF-Cz chain in the spin-coated films. "d" represents the interchain backbone distance in PHDPF-Cz films. "dCz" is the standard π-stacking distance among interchain or intrachain pendent Cz units. The inset also shows an AFM image of the PHDPF-Cz film spin-coated from toluene solution.

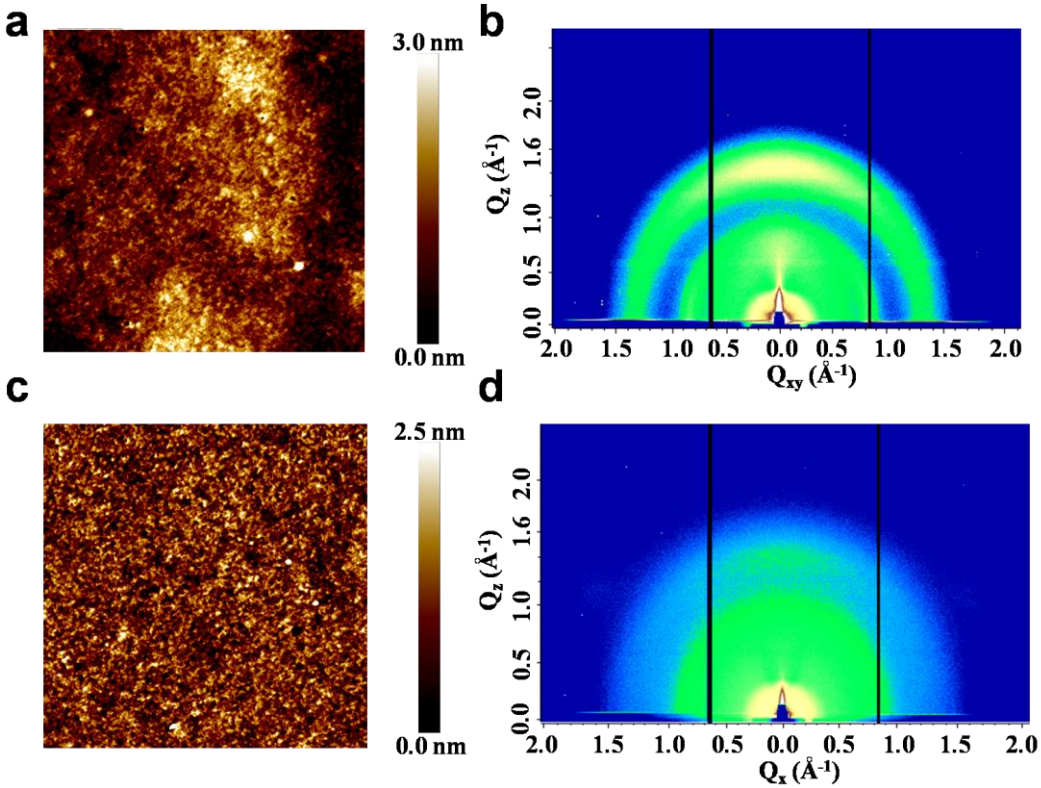

Figure S13. AFM (a) and Grazing-incidence-X-ray scattering (GIXD) (b) images of PHDPF-Cz films spin-coated from $CHCl_3$ solution with the concentration of 10 mg/ml.

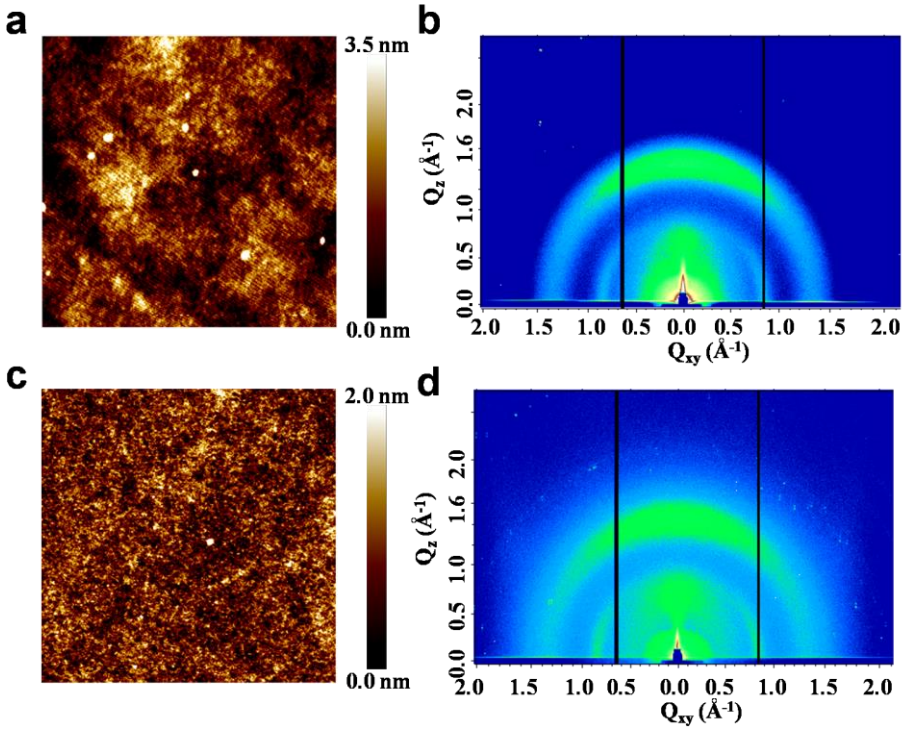

Figure S14. AFM and Grazing-incidence-X-ray scattering (GIXD) images of PHDPF films spin-coated from toluene (a, b) and $CHCl_3$ (c, d) solution with the concentration of 10 mg/ml, together with their AFM images, respectively.

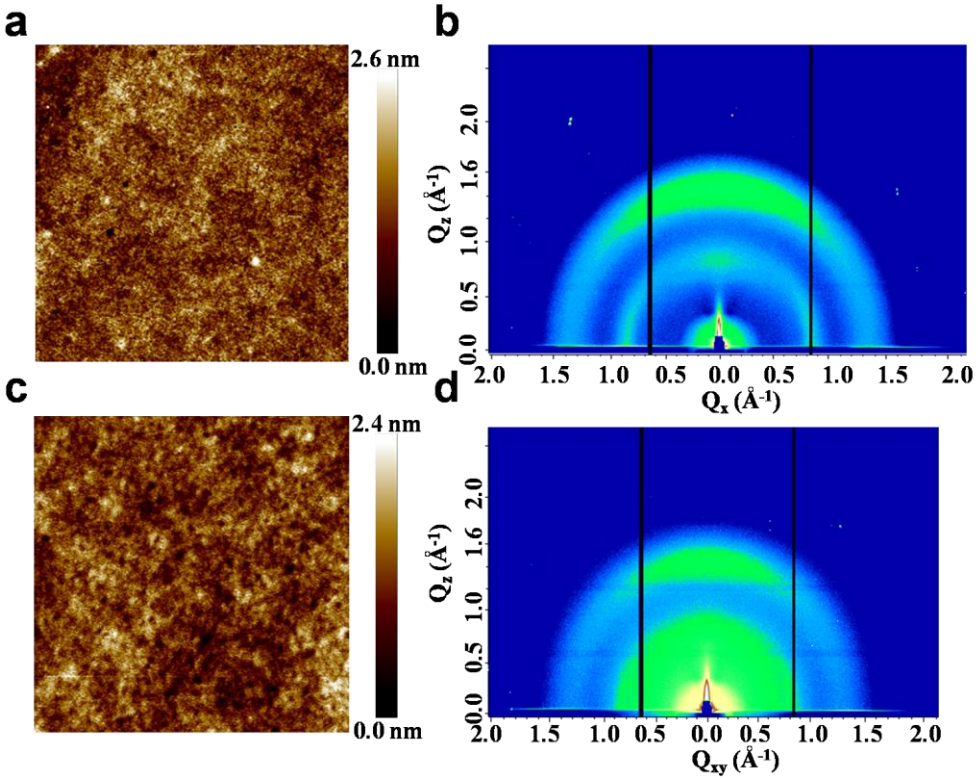

Figure S15. AFM and Grazing-incidence-X-ray scattering (GIXD) images of PNDPF films spin-coated from toluene (a, b) and $CHCl_3$ (c, d) solution with the concentration of 10 mg/ml, together with their AFM images, respectively.

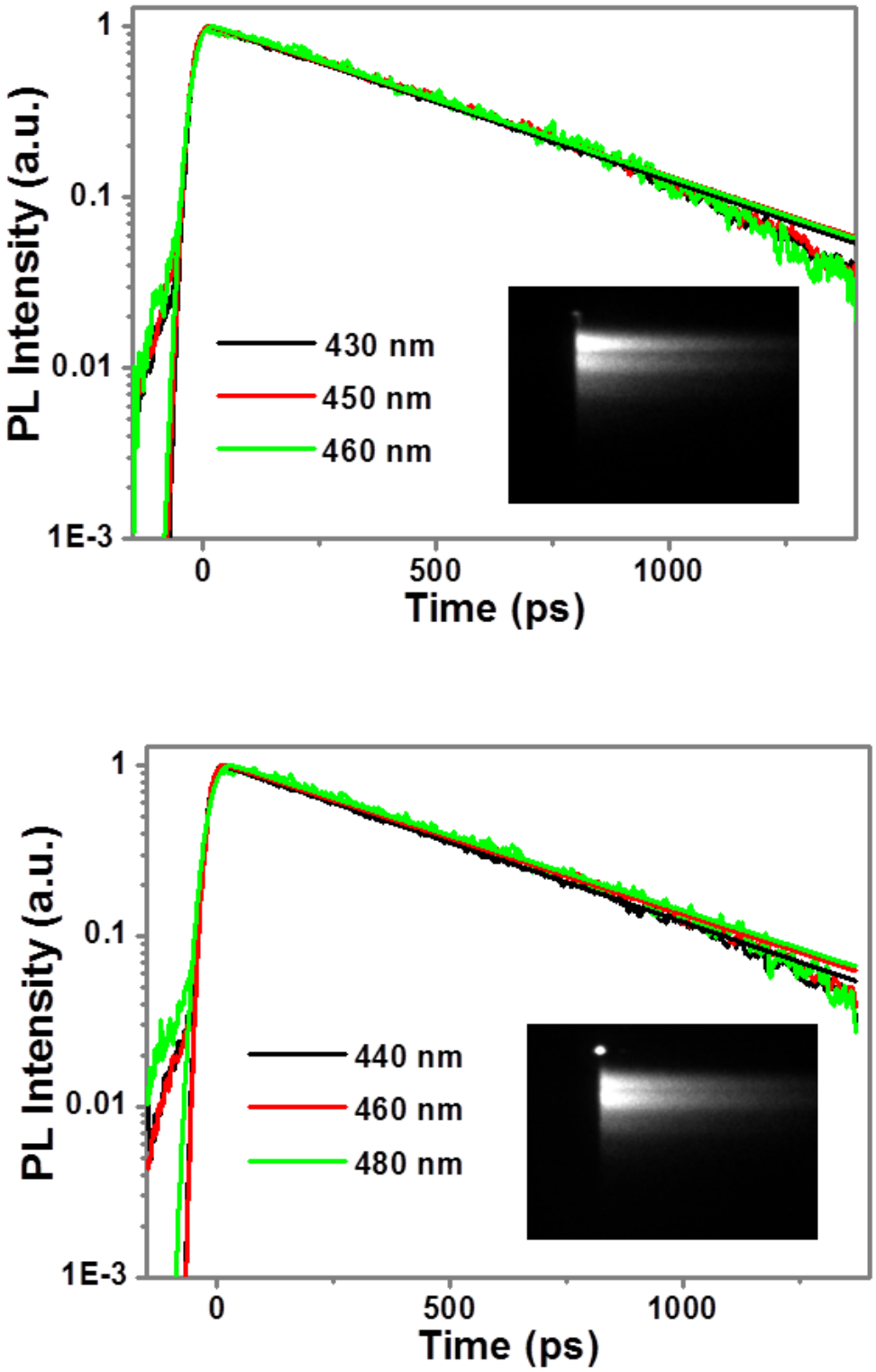

Figure S16. PL decays of the PHDPF-Cz in toluene solution (top) and gels (bottom) at different wavelengths. 2D Time-resolved PL spectra are shown in the inset.

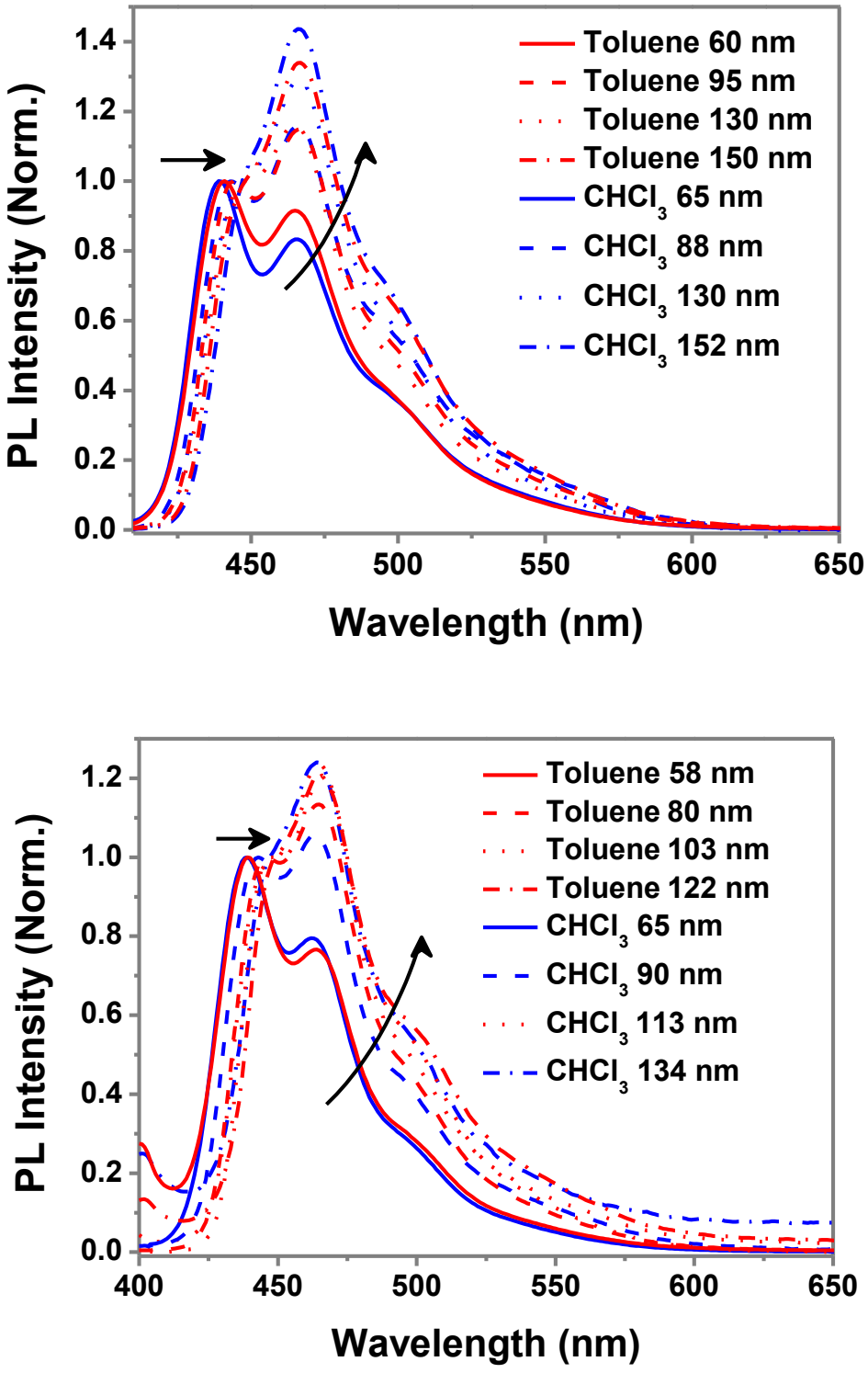

Figure S17. PL spectra of PHDPF (Top) and PNDPF (Bottom) films spin-coated from toluene and $CHCl_3$ solutions with the different thickness.

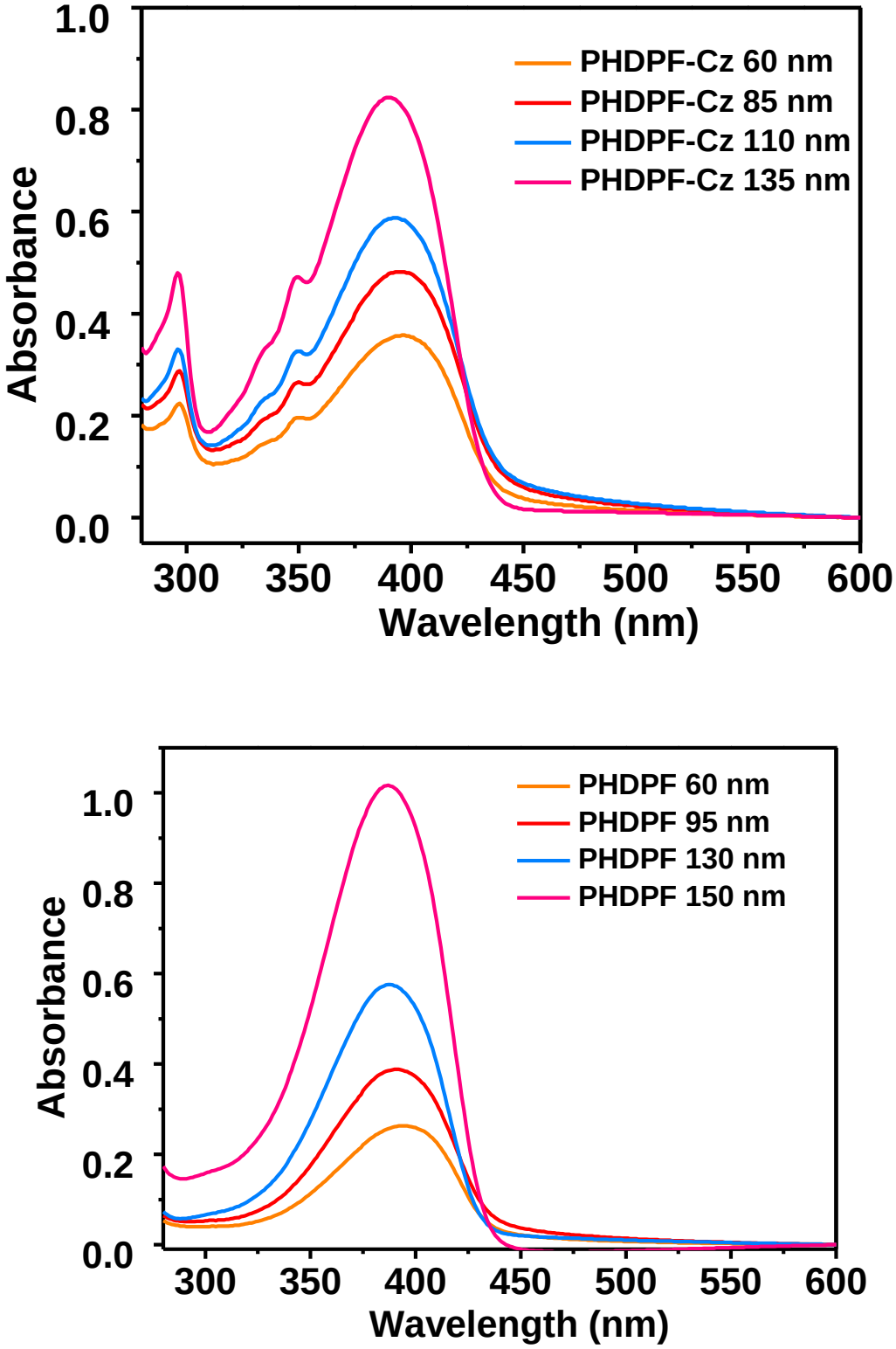

Figure S18. Absorbance spectra of PHDPF-Cz and PHDPF films spin-coated from toluene solutions with the different thickness.

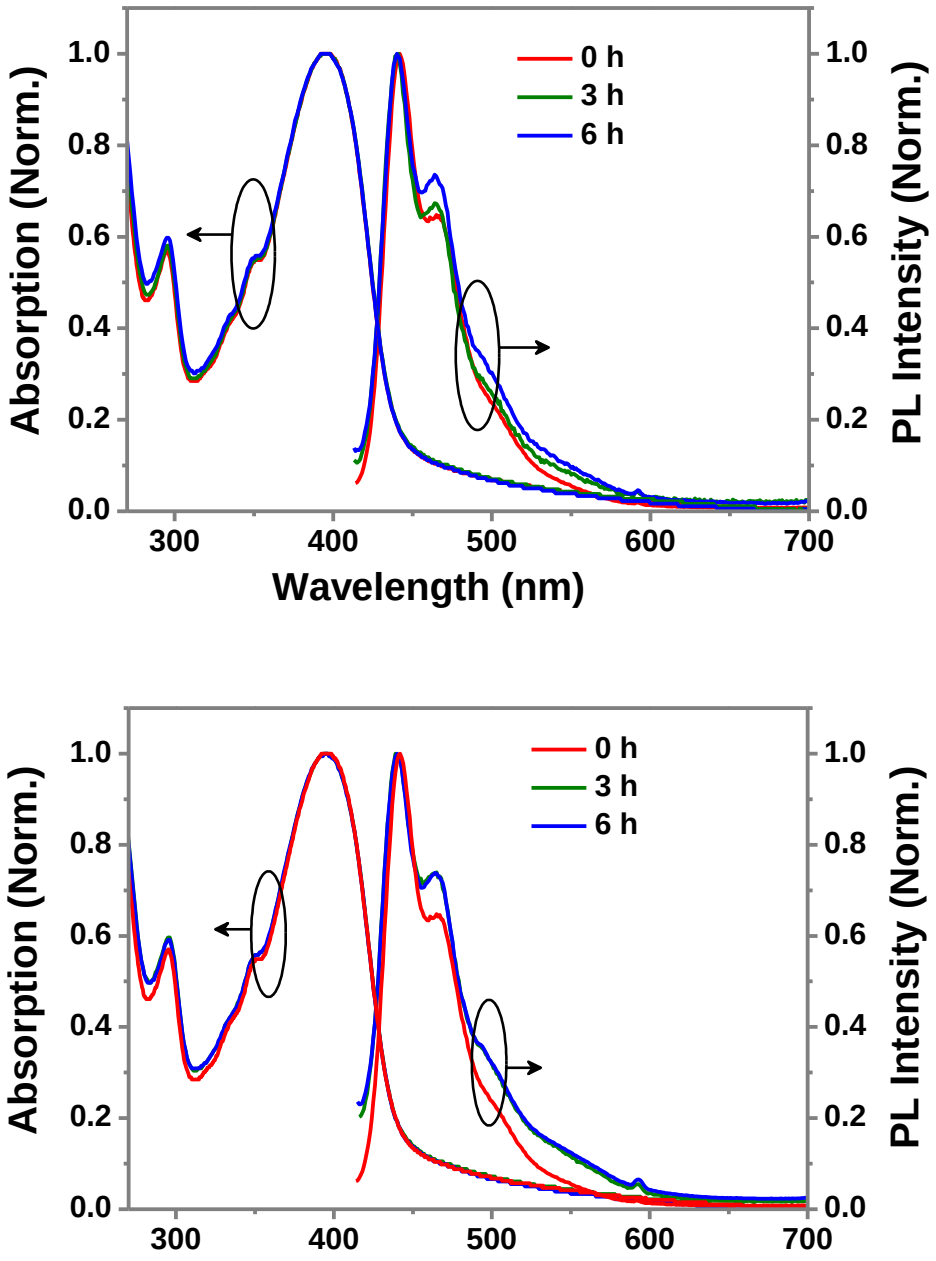

Figure S19. Absorbance and PL spectra of PHDPF-Cz films spin-coating from $CHCl_3$ solution after thermal annealing at 200 °C in N_2 (Top) and in air (Bottom) for 0, 3 and 6 hours. Thickness is about 80 nm.

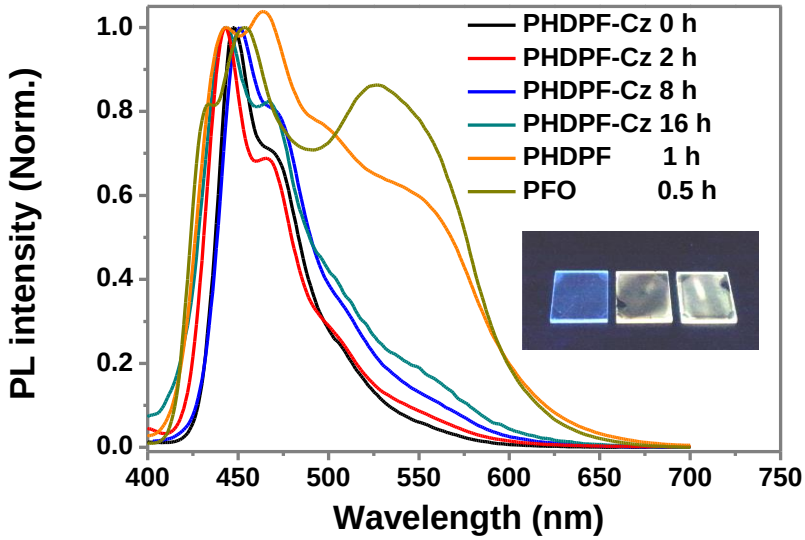

Figure S20. PL spectra of PHDPF-Cz, PHDPF and PFO aged films (all about 90~100 nm) and $CHCl_3$ (all about 95~105 nm). PL spectra of PHDPF-Cz, PHDPF and PFO films spin-coated from toluene with various times under UV lamp in ambient atmosphere (Humidity: 50%, Temperature: 301 K, Daylight.). Insets show the photographs of films keeping under air at 16 h.

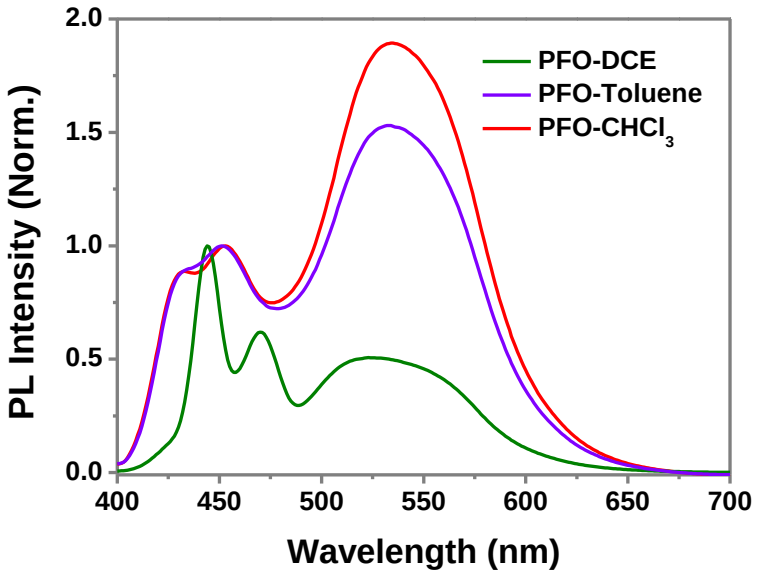

Figure S21. PL spectra of PFO films spin-coated from 1,2-dichloroethane (DCE) (β Phase film, 88 nm), toluene (Amprohous film with lower content of β phase, 85 nm) and $CHCl_3$ (amorphous film, 80 nm) solutions under aging 3 days under the air and daylight.

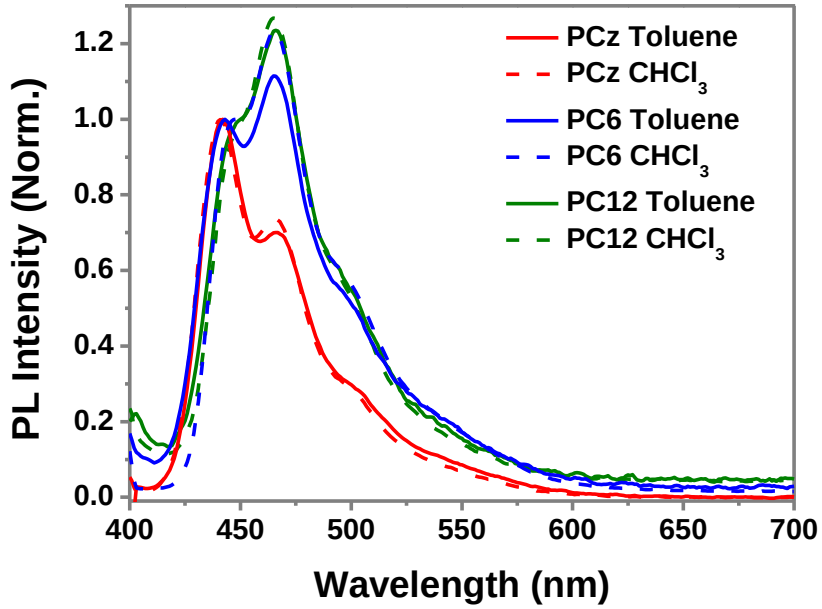

Figure S22. PL spectra of PHDPF-Cz, PHDPF (PC6) and PNDPF (PC12) films spin-coated from toluene and $CHCl_3$ solutions under aging 21 days in the N_2 atmosphere.

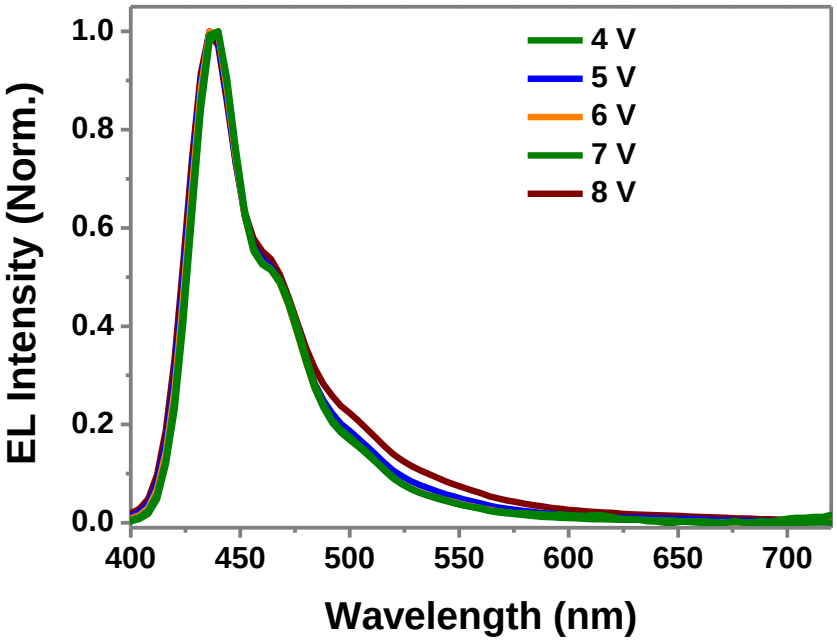

Figure S23. EL spectra of PLEDs based on PHDPF-Cz film spin-coating from toluene solution with the concentration of 6 mg/ml (58 nm).

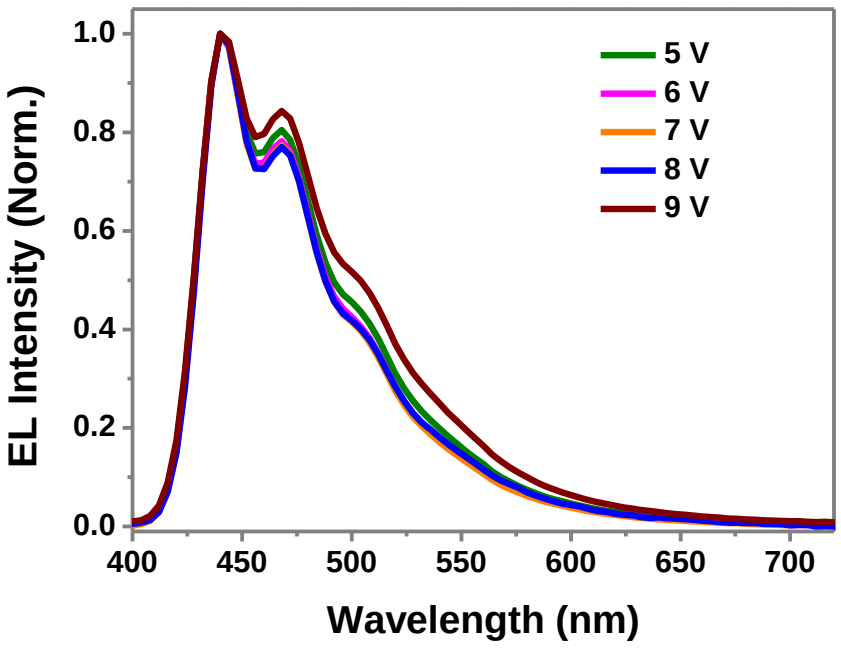

Figure S24. EL spectra of PLEDs based on PHDPF-Cz film spin-coating from $CHCl_3$ solution with the concentration of 10 mg/ml (100 nm).

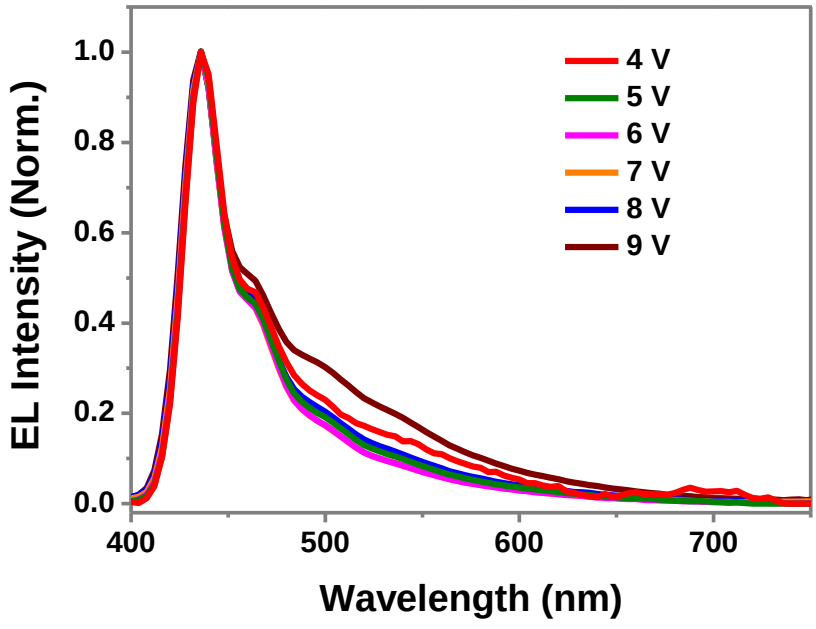

Figure S25. EL spectra of PLEDs based on PHDPF-Cz film spin-coated from $CHCl_3$ solution with the concentration of 6 mg/ml (63 nm).

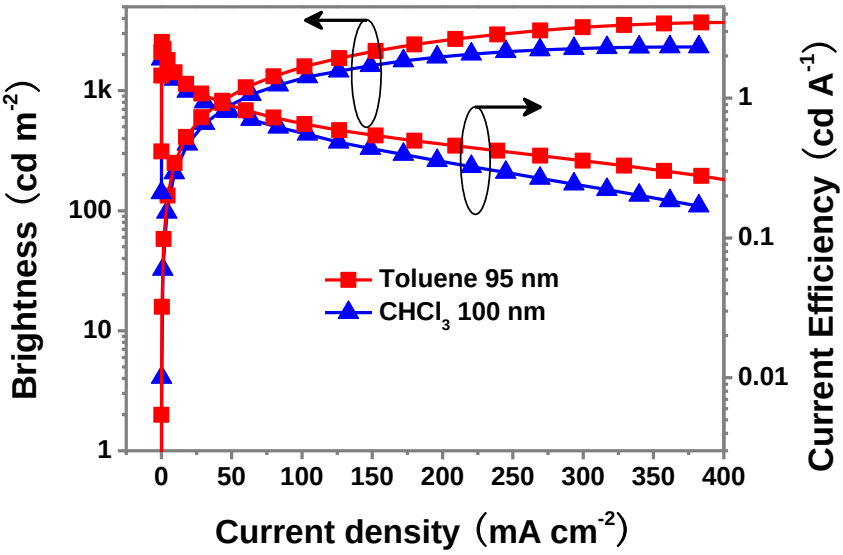

Figure S26. Current-density-brightness-luminous-efficiency characteristics of PLEDs based on PHDPF-Cz films spin-coated from toluene (95 nm) and $CHCl_3$ (100 nm).

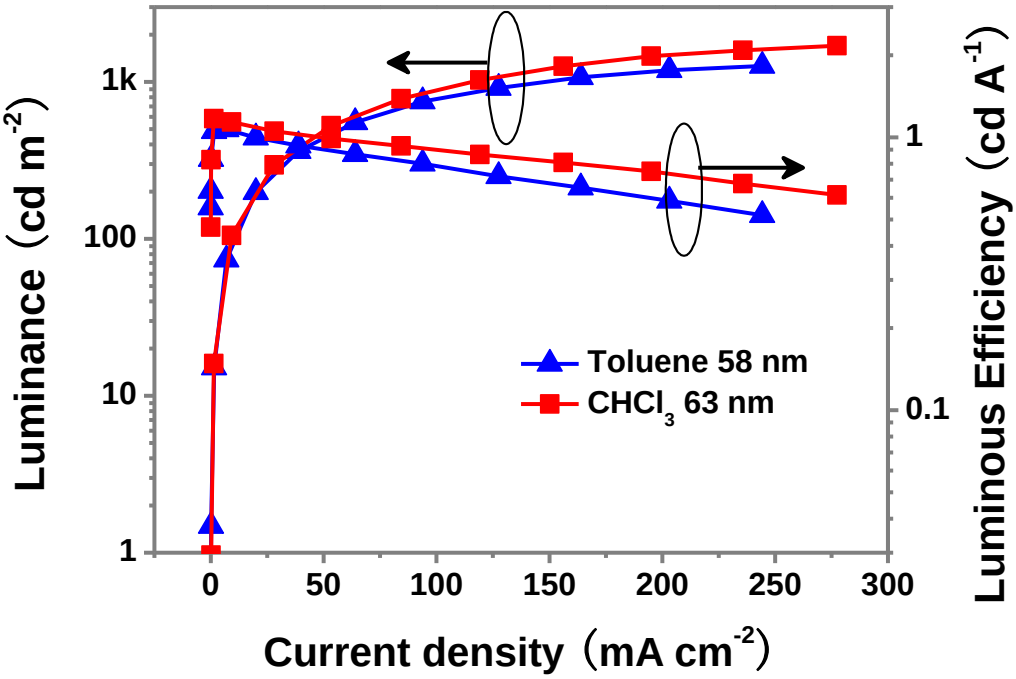

Figure S27. Current-density-brightness-luminous-efficiency characteristics of PLEDs based on PHDPF-Cz films spin-coated from toluene (58 nm) and $CHCl_3$ (63 nm).

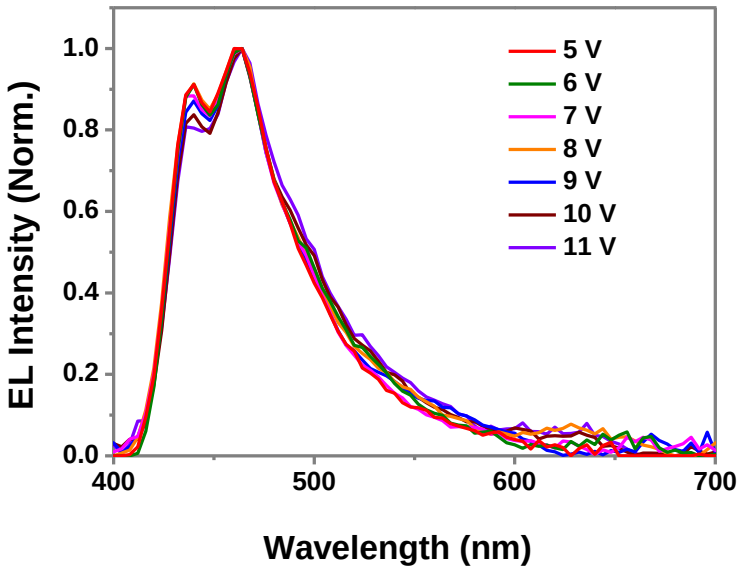

Figure S28. EL spectra of PLEDs based on PHDPF film spin-coating from toluene solution with the concentration of 10 mg/ml (92 nm), similar to PNDPF under the same experimental conditions.

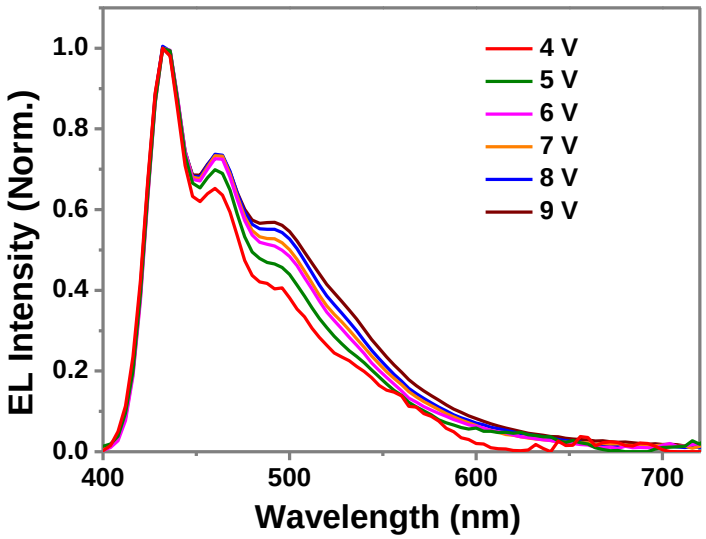

Figure S29. EL spectra of PLEDs based on PHDPF film spin-coated from toluene solution with the concentration of 6 mg/ml (58 nm), similar to PNDPF under the same experimental conditions..

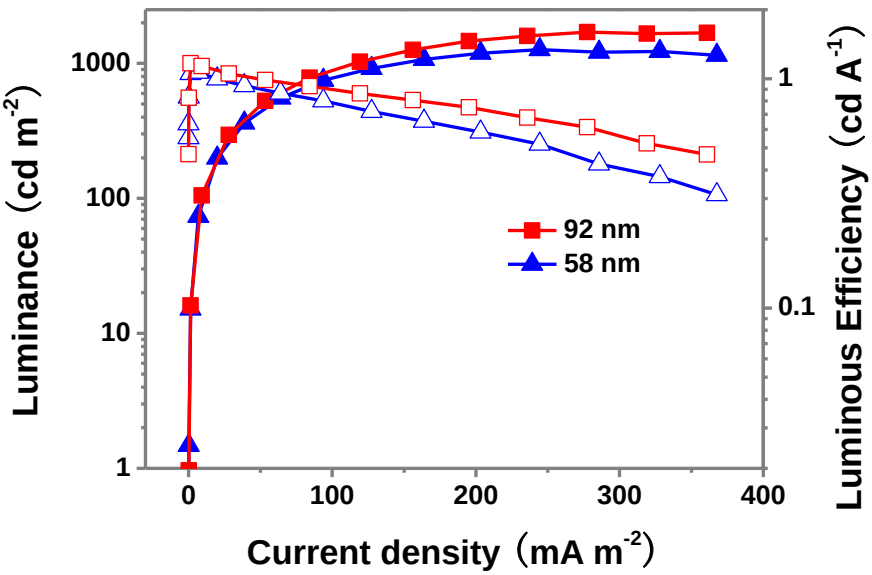

Figure S30. Current-density-brightness-luminous-efficiency characteristics of PLEDs based on PHDPF films spin-coated from toluene with the concentration of 10 mg/ml and 6 mg/ml.

Table S1. The fitting results of PL decay curves as single exponential decay functions.

sample	Wavelength (nm)	A_1	τ_1 (ps)
PHDPF-Cz Solution	433	1	472
	460	1	486
	480	1	480
PHDPF-Cz Gel	440	1	466
	468	1	486
	499	1	491